

## Aircraft observations of thin cirrus clouds near the tropical tropopause

Leonhard Pfister,<sup>1</sup> Henry B. Selkirk,<sup>2</sup> Eric J. Jensen,<sup>1</sup> Mark R. Schoeberl,<sup>3</sup> Owen B. Toon,<sup>4</sup> Edward V. Browell,<sup>5</sup> William B. Grant,<sup>5</sup> Bruce Gary,<sup>6,7</sup> Michael J. Mahoney,<sup>6</sup> Thaopaul V. Bui,<sup>1</sup> and Eric Hints,<sup>8,9</sup>

**Abstract.** This work describes aircraft-based lidar observations of thin cirrus clouds at the tropical tropopause in the central Pacific obtained during the Tropical Ozone Transport Experiment/Vortex Ozone Transport Experiment (TOTE/VOTE) in December 1995 and February 1996. Thin cirrus clouds were found at the tropopause on each of the four flights which penetrated within 15° of the equator at 200–210 east longitude. South of 15°N, thin cirrus were detected above the aircraft about 65% of the time that data were available. The altitudes of these clouds exceeded 18 km at times. The cirrus observations could be divided into two basic types: thin quasi-laminar wisps and thicker, more textured structures. On the basis of trajectory analyses and temperature histories, these two types were usually formed respectively by (1) in situ cooling on both a synoptic scale and mesoscale and (2) recent (a few days) outflow from convection. There is evidence from one case that the thicker clouds can also be formed by in situ cooling. The actual presence or absence of thin cirrus clouds was also consistent with the temperature and convective histories derived from back trajectory calculations. Notably, at any given time, only a relatively small portion (at most 25%) of the west central tropical Pacific has been influenced by convection within the previous 10 days. The structures of some of the thin cirrus clouds formed in situ strongly resembled long-wavelength (500–1000 km) gravity waves observed nearly simultaneously by the ER-2 on one of the flights. Comparison with in situ water vapor profiles made by the NASA ER-2 aircraft provide some observational support for the hypothesis that thin cirrus clouds play an important role in dehydrating tropospheric air as it enters the stratosphere.

### 1. Introduction

Recent work by *Jensen et al.* [1996] has shown that subvisible and horizontally extensive subvisible cirrus

clouds (SVC) near the tropical tropopause can govern the water vapor input into the lower stratosphere by simultaneously removing water vapor by sedimentation and lofting the affected air parcels through enhanced IR radiative heating of cloud particles. The large horizontal extent of SVCs (several 100 km, as shown by *McFarquhar et al.* [2000]) and substantial frequency over large parts of the tropical atmosphere [*Wang et al.*, 1996] implies a role in (1) the thermal balance of the tropical tropopause region and (2) the Earth's overall radiation balance. As shown by *Rosenfield et al.* [1998], cirrus formation may raise the average temperature of the tropical tropopause by 1–2 K. Since such a temperature increase implies an increase in the ice saturation mixing ratio, SVC formation at the tropical tropopause is raising the water vapor input into the lower stratosphere above what it would otherwise be. Recent radiative forcing calculations (E. J. Jensen, personal communication, 2000) show that an atmosphere with a “wet” tropopause (80% relative humidity) has 1 W m<sup>−2</sup> less outgoing longwave radiation than a “dry” tropopause (50% relative humidity), a significant number for net

<sup>1</sup>NASA/Ames Research Center, Moffett Field, California.

<sup>2</sup>Space Physics Research Institute, Sunnyvale, California.

<sup>3</sup>NASA/Goddard Space Flight Center, Greenbelt, Maryland.

<sup>4</sup>Laboratory for Atmospheric and Space Physics, University of Colorado, Boulder, Colorado.

<sup>5</sup>NASA/Langley Research Center, Hampton, Virginia.

<sup>6</sup>Microwave and Lidar Technology Section, Jet Propulsion Laboratory, Pasadena, California.

<sup>7</sup>Now at Santa Barbara, California.

<sup>8</sup>Atmospheric Research Project, Harvard University, Cambridge, Massachusetts.

<sup>9</sup>Now at Woods Hole Oceanographic Institution, Woods Hole, Massachusetts.

Copyright 2001 by the American Geophysical Union.

Paper number 2000JD900648.

0148-0227/01/2000JD900648\$09.00

radiative forcing in global climate studies. Clouds, even thin ones, would substantially enhance this difference.

The potential importance of these clouds to the stratospheric water budget depends on how they are formed. There are two possibilities: excess ice left over from a convective outflow and in situ formation. If they are excess ice left over from a convective outflow (i.e., ice formed in the convective system and passed into the anvil outflow that has failed to fall out because of small particle size), then their role depends on the position of that convective outflow with respect to the tropopause. If they are below the tropopause, they will be radiatively heated, but their temperature will still decrease as the cloud rises in an environment where temperature decreases with altitude [Ackerman *et al.*, 1988]. In this case, the convective outflow ice crystals will continue to grow and presumably fall out, and the clouds will act both to advect moisture upward and simultaneously remove it [Sherwood, 1999]. Given that in situ ice nucleation may require some degree of supersaturation [Koop *et al.*, 1998], the presence of "seed" ice from convection may actually enhance dehydration by allowing ice particles to grow at saturated rather than supersaturated water vapor values. Above the tropopause, the reverse is true. Radiative heating of the convective outflow will simply evaporate the leftover ice crystals and act to hydrate the lower stratosphere. If they are formed in situ (due to temperature changes induced by wave activity or large-scale ascent in the tropopause region), they can be viewed as a mechanism that simultaneously lifts air upward and strips it of water vapor [Jensen *et al.*, 1996]. It should be noted that convective outflow cirrus can also be lifted and cooled by wave activity, leading to net dehydration. The observations documented in this paper indicate the presence of both convective outflow cirrus and cirrus formed in situ. These observations also show that short-term (10 days or less) trajectories near the tropopause based on standard analyses are quite credible even in the data-sparse tropical regions.

## 2. Experimental and Meteorological Background

The Tropical Ozone Transport Experiment/Vortex Ozone Transport Experiment (TOTE/VOTE) was actually designed to examine filaments of stratospheric tracers and assess their role in large-scale lateral mixing in the tropics and polar regions. To examine these filaments, NASA's DC-8 aircraft was equipped with a number of in situ and remote instruments, including a UV Differential Absorption Lidar (UVDIAL) [Browell *et al.* 1983, 1998] measuring aerosol backscatter, aerosol depolarization, and ozone, and a Microwave Temperature Profiler (MTP) [Denning *et al.* 1989; Gary, 1989], measuring the temperature profile between ~5 km and ~25 km altitude along the aircraft flight track. The experimental protocol called for the aircraft to fly at maximum cruise altitude (~11 km) at night (to maximize

lidar signal to noise ratios) and make measurements in a vertical profile between the aircraft and maximum instrument altitude (~25 km for UVDIAL ozone and MTP temperature). Though an investigation of high-altitude cirrus clouds was not an initial central goal, this experiment was unique in high-altitude cirrus investigations in two ways. First, it provided, simultaneously, cloud information (the total scattering ratio (TSR) and depolarization at 603 nm from the UVDIAL) and temperature information (MTP). Second, for one of the flights, in situ data from a NASA ER-2 aircraft was available nearly simultaneously; that is, the ER-2 flew along essentially the same track ~16 hours after the DC-8.

The tropical portions of TOTE/VOTE took place in two phases, December 13–20, 1995, and February 13–17, 1996. During these two periods, there were six local flights out of Hawaii: four were directed southward reaching the equator, one spanned the latitude range 13°–28°N with Hawaii as the midpoint, while one was directed northwestward of Hawaii. Figures 1a and 1b show the flight tracks of the four equatorial flights superimposed on the average brightness temperature during the December 1995 and February 1996 periods. Consistent with longer-term climatologies (e.g., ISCCP, [Rossow and Schiffer, 1991]), the region south of Hawaii is relatively free of deep high clouds. The areas of colder average brightness temperatures coincide with three general regions of tropical deep convection. For this period, these are, in decreasing order of overall convective activity, (1) a broad, region of extensive convection over Indonesia, northern Australia, and the eastern Indian ocean; (2) a line of convective activity in the Southern Hemisphere with a slight northwest-southeast tilt extending from Indonesia eastward across the international dateline towards American Samoa and south of Tahiti, also known as the Southern Pacific Convergent Zone (SPCZ); and (3) a narrow, fairly weak InterTropical Convergent Zone (ITCZ) extending eastward through the international dateline near 7°N.

Also plotted in Figures 1a and 1b are the average wind fields and temperatures at 85 hPa (slightly above the tropopause level). Of note for this study is the monsoon anticyclone in the Northern Hemisphere extending from the equator to the subtropical jet edge near 20°N and from ~90°E to Hawaii [Allam and Tuck, 1984]. Outflow from region 1 convection flows (in part) northward toward the subtropical jet. It is then carried eastward by that jet and returns to the equator in a broad region of longitudes centered roughly at the Hawaiian islands. Whereas the convective outflow and the subtropical jet west of the dateline are fairly steady, the return flow fluctuates substantially as amplifying waves travel along the subtropical jet, slow down as the jet weakens in the eastern Pacific, and "dig" equatorward. Along the equator, between Hawaii and the Indonesian convective region, the flow is westward, completing the anticyclone. A similar monsoon anticyclone is found in the

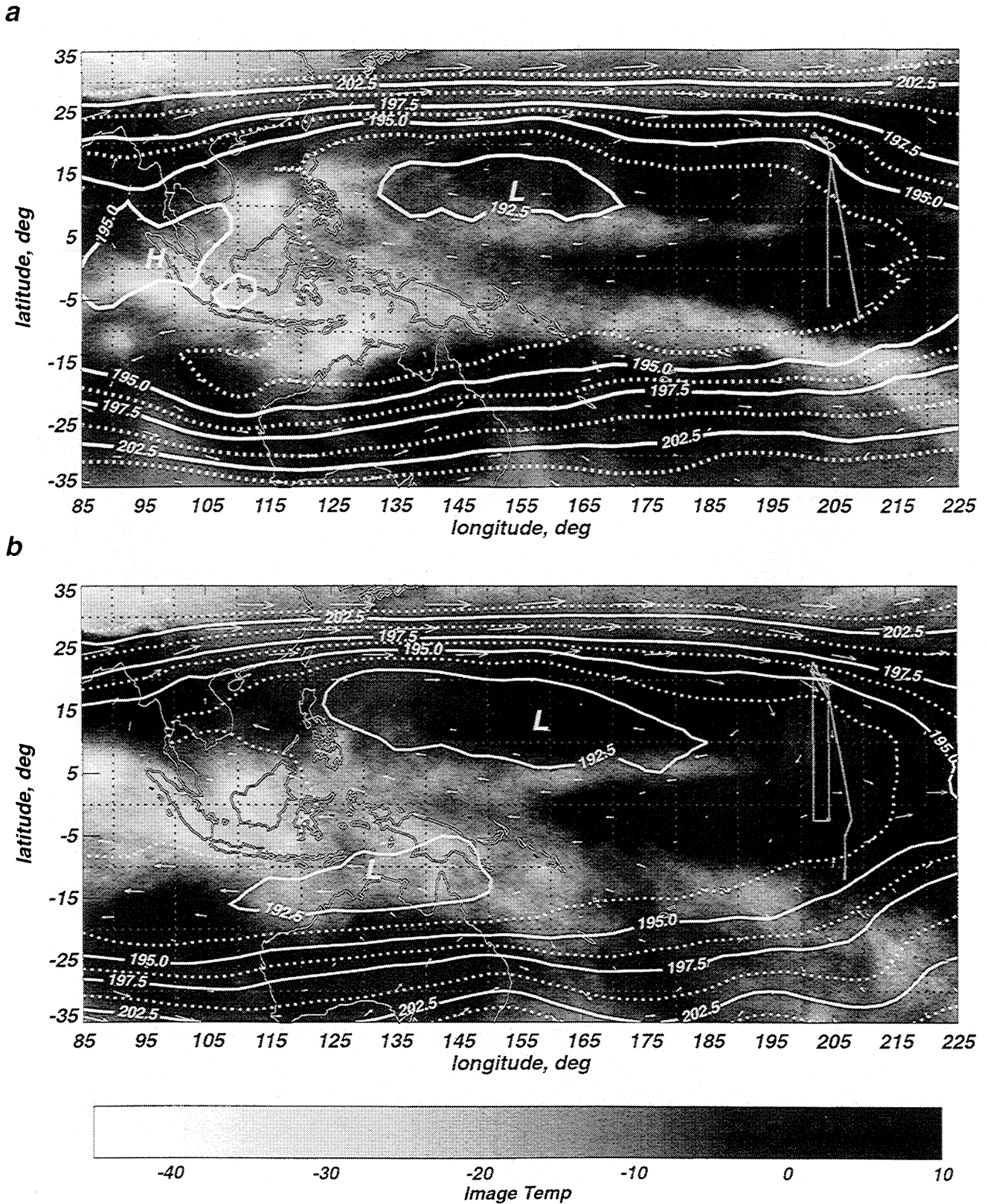


**Figure 1.** Average 10.5 micron brightness temperature as observed by the GMS-5, GOES-7, and GOES-9 meteorological satellites during two periods of winter 1995-1996: (a) December 5-25, 1995 and (b) February 1-19, 1996. Average winds and temperatures on the 85 hPa surface for both periods from NASA GSFC GEOS-1 analyses are superimposed.

Southern Hemisphere, centered roughly over the Australian continent [Danielsen, 1993; Kelly *et al.*, 1993]. At Hawaiian longitudes, however, between the SPCZ and the equator, there is a weak northeastward flow which meets the southward branch of the northern anticyclone in a diffluent region near the equator. The temperature field shows that the coldest tropopause temperatures are centered near 12°N, 150°E, and do not, in fact, coincide with the regions of strongest convection. Thus outflow from Indonesian convection may actually cool somewhat as it passes northward, then warm as it approaches the subtropical jet. In the return flow near Hawaiian longitudes, the air will cool substantially as it approaches the equator.

### 3. Observations

High altitude cirrus (HAC) were observed on all four southward flights and very briefly on the Hawaii mid-point flight south of 15°N. The HAC were generally south of 15°N, extending as far north as 18°N on the flight of 951215 (year, month, and day). Here we define thin cirrus as follows: (1) TSR greater than 1.175, (2) 603 nm depolarization greater than 0.3, and (3) no evidence of high cloud (above the DC-8) based on the 6.5 and 10.5 micron channels from the geostationary meteorological satellite imagery. Criterion (1) indicates the presence of a layer of particles distinct from the stratospheric aerosol (which has lower TSRs) and criterion (2) indicates that the degree of nonsphericity of those particles is sufficiently high to show the presence of ice [Browell *et al.*, 1983]. Criterion (3) is a crude measure of optical depth; if it is met, whatever clouds are present are too thin to be detected by nadir sounders. Note here that the use of the term “subvisible cirrus” is avoided, since that term implies a maximum optical depth of 0.03 [Sassen *et al.*, 1989], a quantity that cannot be unambiguously determined from the available data. With few exceptions, the aircraft flew in nearly cloud free zones (essentially by design in order to allow the lidar instruments to make stratospheric observations).

Figures 2a-2e show latitude-altitude cross sections of the TSR observed by the DC-8 on the four equatorial Hawaii flights. Only the southbound legs are shown for the three flights where the inbound legs coincided with the outbound legs (951215, 951220, and 960217). Also plotted are the temperatures from the Microwave Temperature Profiler [Denning *et al.*, 1989] and the potential temperatures from the NASA Goddard Space Flight Center GEOS-1 Assimilation Model [Schubert and Rood, 1993]. Note that in this and all subsequent figures, “altitude” refers to standard pressure altitude, equal to geometric altitude for a U.S. standard atmosphere temperature profile. Near the tropical tropopause, the geometric altitude is ~0.5 km higher than the standard pressure altitude. The corresponding nadir sounding images are in Figures 4a-4d (10.5

micron channel), which clearly show that all four flight tracks were in substantially cloud-free regions.

The aircraft essentially ascended in steps as fuel was burned, and these upward steps are indicated by the upward steps in the lower limit of the TSR data. Three general features of the observations are to be noted. First the HAC are clearly confined in altitude to the region within 2 km of the temperature minimum (presumably the tropopause), as shown by the MTP measurements. Second the HAC seem to have two basic types. The first (HAC1), as exemplified by the observations for the flight of 960213, the flight of 951220 north of 6°N, and the flight of 951215 north of 10°N, are fairly uniform over large horizontal distances and have low TSRs (less than 3) and small aspect ratios (their thickness to length ratio is 0.001 or less). They are also tilted, having a distinct slope of ~0.001 for the HAC near 12°N on 951220 and somewhat higher for 960213. Most of the tilted clouds sloped upward and poleward. However, on the northbound leg of the 960213 flight, there is an opposite slope between 1°-4°N near 16 km. The second type, exemplified by the flight of 960217, the flight of 951220 south of 3°S, and the flight of 951215 south of 10°N, has a blobbier, vertically thicker structure with no apparent slope (HAC2). The maximum TSRs are larger than for HAC1, reaching 1000 for the HACs during the flight of 951215. The third general feature, not shown, is that all of the regions of enhanced TSR had significant depolarization, indicating that these were ice clouds with nonspherical particle shapes. Table 1 summarizes the locations and times that the two types of HAC were observed.

Figure 3 shows the fractional incidence of HAC south of 15°N as a function of altitude for each of the four flights, plus an overall average. Note that the lidar observations have a minimum altitude which varies from flight to flight. These data cutoffs are apparent in Figure 2 (the horizontal white lines below which there are no contours) and show as zero values below 15-16 km in Figure 3. The overall average values are set to zero below 15.3 km, the highest data cutoff point for the four flights. The statistical significance of the maximum near 16.2 km is marginal because of flight-to-flight variability. The decrease with altitude, however, is reliable, with significant incidence extending up to 18 km. For comparison, Kelly *et al.* [1993] showed ice extending up to ~403 K, or ~17.6 km. The overall values indicate 35% coverage near 16.2 km. Since many of the clouds are sloped, the fractional incidence of any overhead HAC at a given horizontal position is higher, ranging from about half (951220) to three quarters (960217), with an overall average of ~65%. Since these flights are in a region that is at the edge of the West Pacific cold pool (Figure 1), higher values in the broad center of the cold pool to the west could be expected, as suggested by the SAGE climatology compiled by Wang *et al.* [1996]. However, in view of the substantial year-to-year vari-

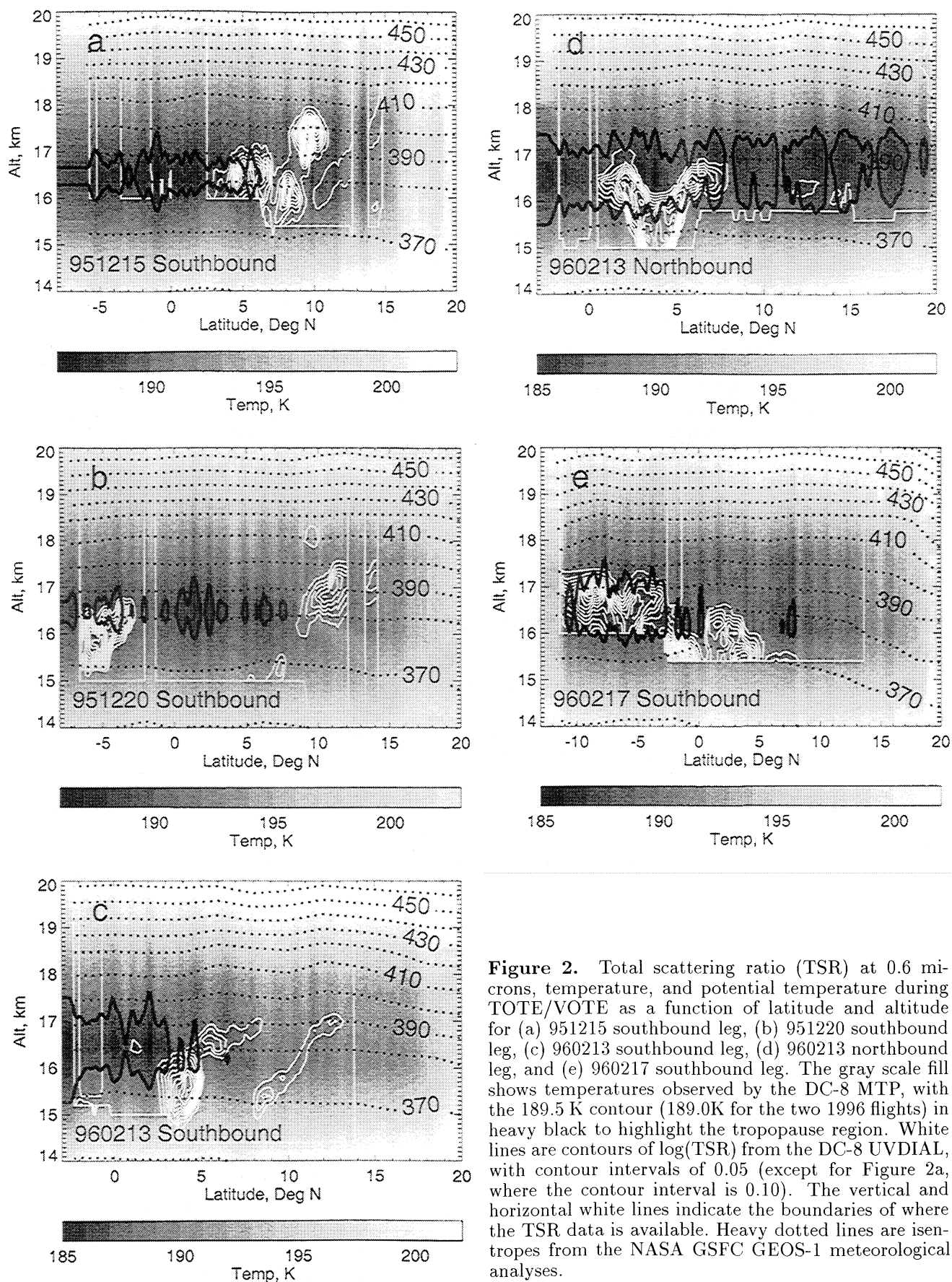


**Figure 2.** Total scattering ratio (TSR) at 0.6 microns, temperature, and potential temperature during TOTE/VOTE as a function of latitude and altitude for (a) 951215 southbound leg, (b) 951220 southbound leg, (c) 960213 southbound leg, (d) 960213 northbound leg, and (e) 960217 southbound leg. The gray scale fill shows temperatures observed by the DC-8 MTP, with the 189.5 K contour (189.0 K for the two 1996 flights) in heavy black to highlight the tropopause region. White lines are contours of log(TSR) from the DC-8 UVDIAL, with contour intervals of 0.05 (except for Figure 2a, where the contour interval is 0.10). The vertical and horizontal white lines indicate the boundaries of where the TSR data is available. Heavy dotted lines are isentropes from the NASA GSFC GEOS-1 meteorological analyses.

**Table 1.** Times and Locations of Observed High-Altitude Cloud Types

| Cloud Type | Flight Date | Latitude Locations |
|------------|-------------|--------------------|
| HAC 1      | 951215      | 10°N–15°N          |
|            | 951220      | 6°N–16°N           |
|            | 960213      | 0°N–13°N           |
|            | 960217      | none               |
| HAC 2      | 951215      | 2°N–11°N           |
|            | 951220      | 7°S–3°S            |
|            | 960213      | none               |
|            | 960217      | 11°S–8°N           |

ability in HAC incidence noted by *Mergenthaler et al.* [1999], the overall significance of these incidence values is largely suggestive.

The observations also have some significant limitations, which make it difficult for this data set to answer a question relevant to *Jensen et al.*'s [1996] mechanism; namely, do these clouds occur above the tropopause? Unfortunately, because of the distance between the aircraft and the tropopause at these latitudes, the tropopause altitude yielded by the MTP is insufficiently precise to establish whether these clouds are unambiguously above the tropopause. Figure 2d, for example, clearly shows an upward step in the position of the minimum temperature that coincides with a step ascent by the aircraft near 6°N. Since the accuracy of the tropopause altitude improves with the closeness of the MTP to the tropopause, we can say that the actual altitude of the minimum temperature point is probably higher than the MTP indicates. On this basis, all the thin cirrus observed on these four flights, with the possible exception of the example near 18 km at 13.5°N on 951215, are at or just below the tropopause.

There are two other aspects of the MTP measurements that are clearly reliable and important for the present study. First, there are clearly significant mesoscale (horizontal scales of 100 km or less) fluctuations evident in the temperature contours in Figure 2. These fluctuations imply that an air parcel may experience peak-to-peak temperature changes on the mesoscale of 5 K or more (B. Gary, personal communication, 1999). Second, in spite of its shortcomings in measuring the position and temperature of the tropopause accurately, the MTP does show that the GEOS-1 analyses clearly overestimate the tropopause temperature. Comparison of GEOS-1 data with ER-2 in situ temperatures (not shown) indicate that though GEOS-1 tropopause positions are correct to ~0.5 km, temperatures are too warm by ~3 K.

With the possible exception of the HAC2s observed during the 951220 and 960217 flights near the south end of the flight track, the HACs were clearly quite far from any active convection reaching the tropopause (see Figures 4a–4d). Thus it is useful to use trajec-

tory analysis to investigate the thermal and convective history of the air parcels in which the HACs are embedded. In particular, we would like to know (1) what is the relationship of the HACs to convective outflow, (2) what is the lifetime of HAC that originate or appear to originate from convective outflow, (3) what is the relationship of the observed HACs to the temperature history, (4) can HACs form from clear, uncloudy air, and (5) if so, how? The convective history of the air establishes whether convective systems high enough to reach the levels at which the HACs were observed affected the air parcels, and if so, when that occurred. The thermal history of the air indicates whether a cloud formed by convective injection can survive until the observation point is reached. It can also provide an indicator, through the minimum temperature encountered during the trajectory history, of what the maximum water vapor content of the air might be, and how close the large-scale temperatures at the point of observation are to saturation. If, for example, a parcel has encountered substantially colder large-scale temperatures in the past than those observed currently, one would not expect to observe large- or synoptic-scale clouds. Clouds should either be absent or require mesoscale cooling to form.

#### 4. Trajectory Analysis Method

On the basis of Figure 2, all the observed HAC have a significant presence on the 380 K surface; thus we will seek to answer the science questions posed above by calculating 10-day adiabatic back trajectories on that isentropic surface from a dense set of points along and adjacent to the DC-8 flight track for each of the four flights. It should be noted that the actual 380 K surface in the tropics at this time of year is ~0.5 km lower than the GEOS-1 analyses indicate. This is due to the

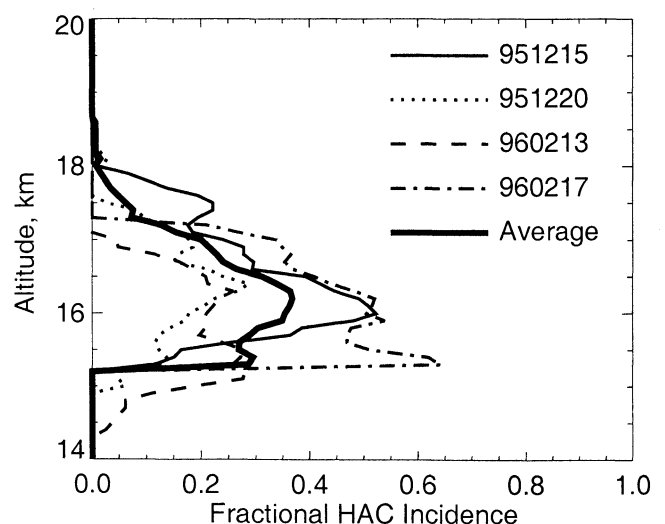


**Figure 3.** Fractional HAC incidence for all four flights, along with an overall average. Details are given in the text.

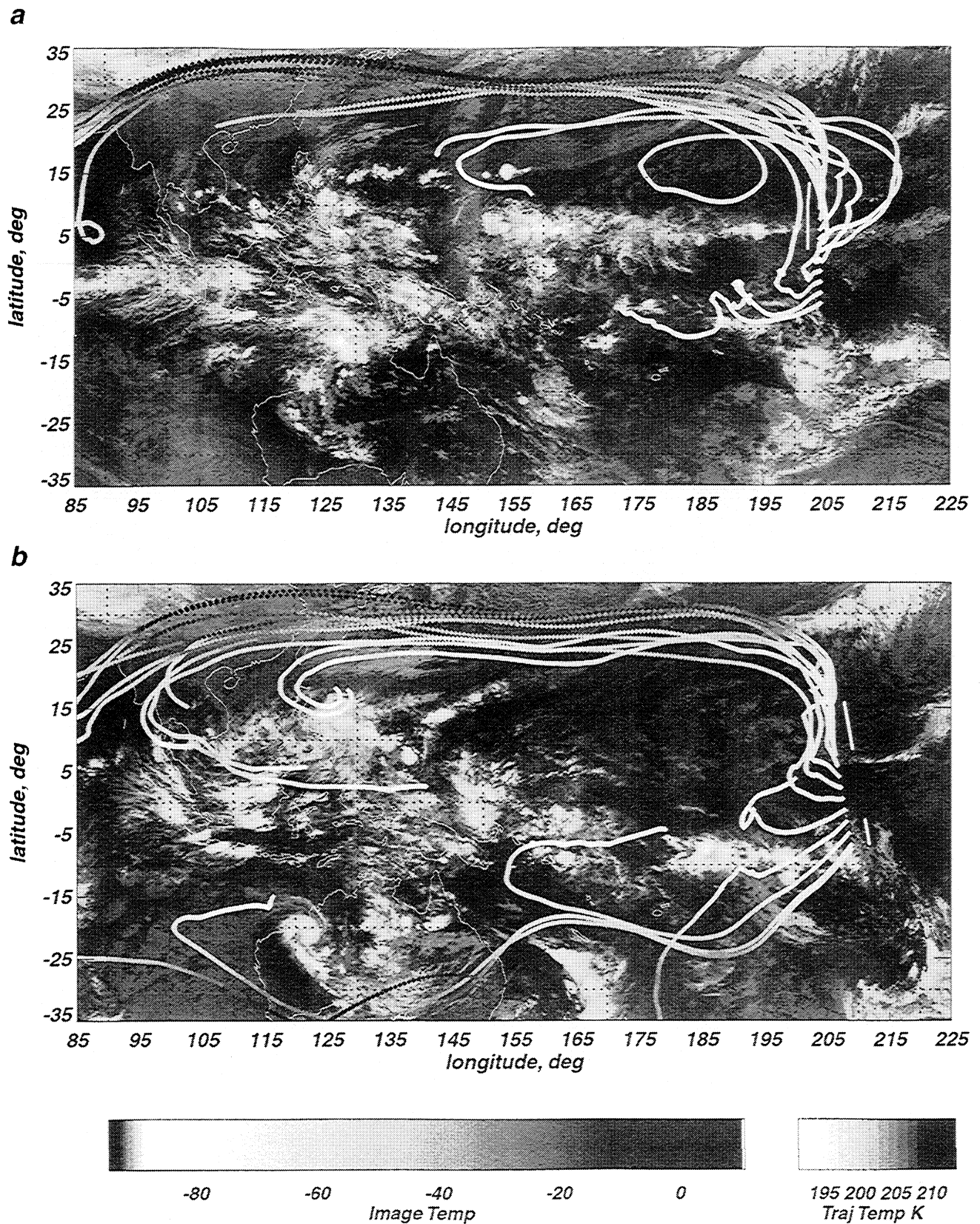


**Figure 4.** Back trajectories on the 380 K surface from selected points along the DC-8 flight track for the flights of (a)951215, (b)951220, (c)960213, and (d)960217. Temperature histories are gray-scale coded along the trajectories. The back trajectories are superimposed on the 10.5 micron brightness temperature images valid at the approximate flight times of the two flights.

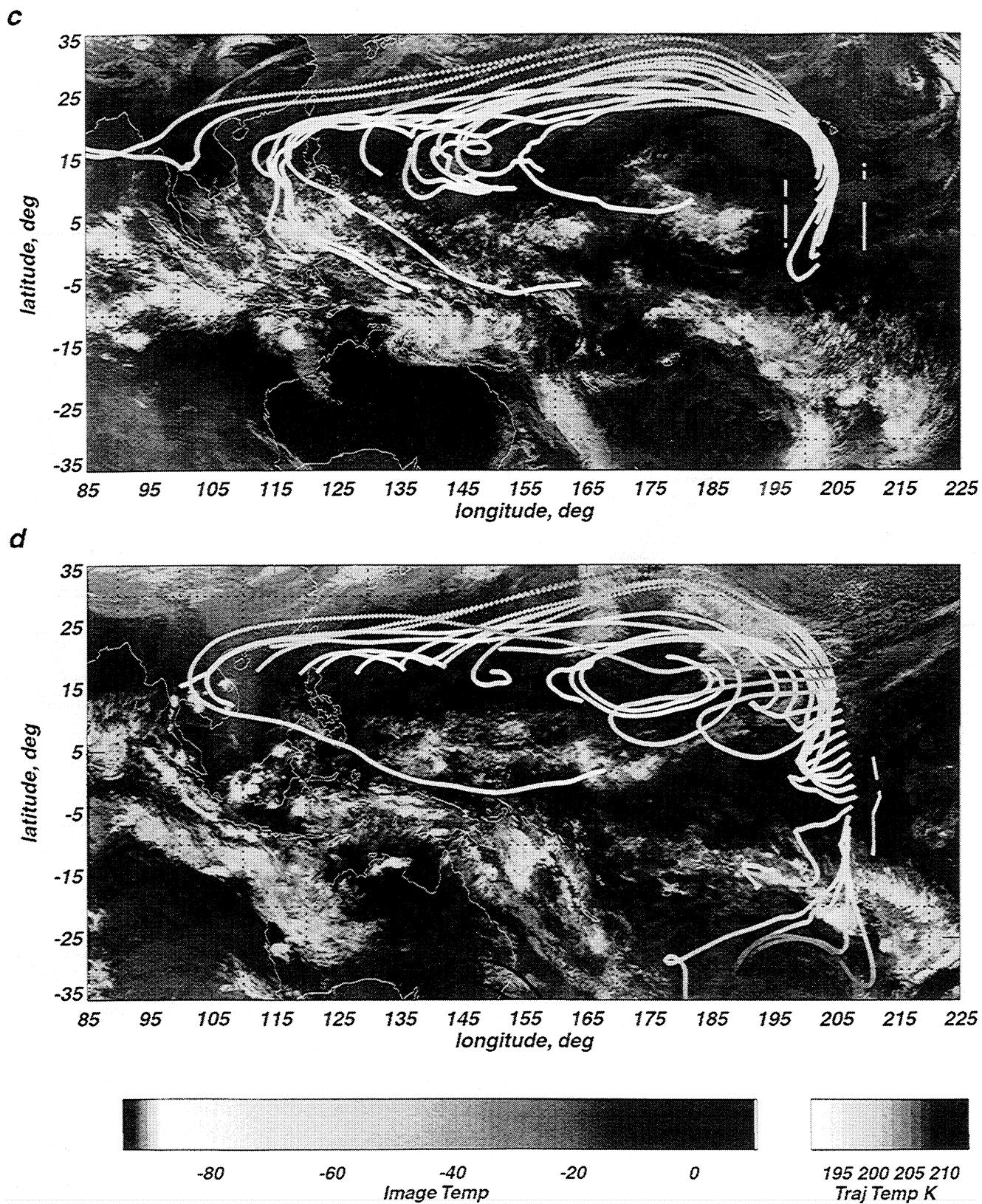


Figure 4. (continued)

fact that the limited vertical resolution of the analyses ( $\sim 1.5$  km at these levels) “rounds out” the sharp tropical tropopause, resulting in tropopause temperatures (and potential temperatures) that are systematically too high. Tropical tropopause locations (in pressure), however, are very reasonable. Since the clouds are located near the tropopause, it is best to choose an isentropic surface that is also near the GEOS-1 model tropopause.

The trajectory model used is that of *Schoeberl and Sparling* [1995], and it is coupled to the GEOS-1 analysis fields, available at 6 hour intervals. The 10-day limit is chosen because radiative heating and cooling in the tropical tropopause region place limitations on the length of time over which a trajectory calculation is valid. *Jensen et al.*, [2000] estimate that the radiative heating rate at the tropical tropopause is  $\sim 0.5$  K  $d^{-1}$ . Such a heating rate changes the potential temperature of a parcel by  $\sim 10$  K in 10 days. Since this is the approximate potential temperature change over the depth of the observed HACs, as shown by Figure 2, this is a reasonable vertical “spread of uncertainty” in the trajectories.

To evaluate the convective history, the temperature along each trajectory is compared to 3-hourly brightness temperatures from the 10.5 micron channel of the GMS-5 and GOES-7 (December, 1995) and GOES-9 (February, 1996) geostationary meteorological satellites. If the brightness temperature is less than or equal to the parcel temperature along the trajectory, we assume that the convective cloud has reached high enough and attained temperatures cold enough to interact with the parcel on the trajectory. This interaction would take the form of a convective anvil outflow into that air parcel. This approach almost certainly underestimates the ability of convective clouds to “influence” the back trajectories, since it implicitly assumes that the brightness temperature is equal to the cloud top temperature (the cloud top temperature then determines the cloud top altitude via the analysis temperature profile). In fact, brightness temperature will always be somewhat warmer than the actual cloud top temperature, since some radiation from warmer underlying surfaces will penetrate through the very top of the cloud. The difference between cloud top temperature and brightness temperature is negligible for the core of the convective cloud [*Liou et al.*, 1990] but may be significant for the outer parts of the anvil. We use a simple approach to correct for this effect. The size of typical convective systems is of the order of  $1^\circ$  by  $1^\circ$ . Since tropical anvils have a roughly constant cloud top altitude [*Danielsen*, 1993], we assume that the brightness temperature at any position in a typical  $1^\circ$  by  $1^\circ$  square is actually equal to the minimum brightness temperature in that square, provided that there is significant cloud at that position. Significant cloud is defined as a brightness temperature of less than 240 K, equivalent

to an optically thick cloud with an altitude of about 9 km. This effectively “flattens” the brightness temperatures for large convective systems, resulting in a more realistic picture of the actual cloud top temperature.

Even including this correction, the impact of convection on large-scale trajectories may still be underestimated. Diabatic radiative heating rates are not large at the tropical tropopause (0.5 K per day, as indicated above). However, these are clear sky calculations. *Ackerman et al.* [1988] have shown that moderately thick anvils have heating rates of the order of 18–20 K per day, effectively raising the potential temperature of the anvil at a rate of about 34 K per day (or 1.4 K per hour). With a lifetime of 5 hours [*Sherwood*, 1999], this implies a potential temperature change of  $\sim 7$  K. Such a change in the potential temperature of the anvil will have one of three effects on the anvil and its environment: (1) a change in the temperature of the anvil (and the environmental temperature profile) with no change in the anvil altitude, (2) a change in the anvil altitude with no change in the anvil temperature or environmental temperature profile, or (3) some combination of (1) and (2). A scale analysis by *Ackerman et al.* [1988] suggests that most of this heating and potential temperature change in the anvil will exhibit itself as anvil ascent in an environment in which the temperature profile remains roughly unchanged. Thus the anvil will actually cool as it follows the decreasing temperatures of the existing temperature profile [*Sherwood*, 1999]. Typically, lapse rates in the tropical upper troposphere between 150 hPa and the tropopause vary from about 7 K  $km^{-1}$  to 4 K  $km^{-1}$ . This is equivalent to positive vertical potential temperature gradients between 5 K  $km^{-1}$  and 10.5 K  $km^{-1}$ . Thus, a potential temperature increase of 7 K for an anvil would imply a temperature decrease between 10 K (for the 7 K  $km^{-1}$  temperature lapse rate) and 3 K (for the 4 K  $km^{-1}$  lapse rate). Thus convective clouds that initially reach somewhat lower altitudes and warmer temperatures than the parcels along a back trajectory can, due to rapid anvil heating during the short period in which they are optically thick, actually reach those back trajectory parcels and inject air and ice particles into them. In view of this radiatively forced ascent, we shall assume that convective interaction occurs along a trajectory when the brightness temperature is less than 10 K warmer than the parcel temperature. On the basis of observed lapse rates, this should represent the largest amount of convective influence that we would expect along a trajectory.

## 5. Results

Figures 4a–4d show a sample of the temperature history of 10-day back trajectories on the 380 K surface superimposed on the brightness temperature images at the approximate flight times of the four flights. The gray scale along the trajectories shows the temperature

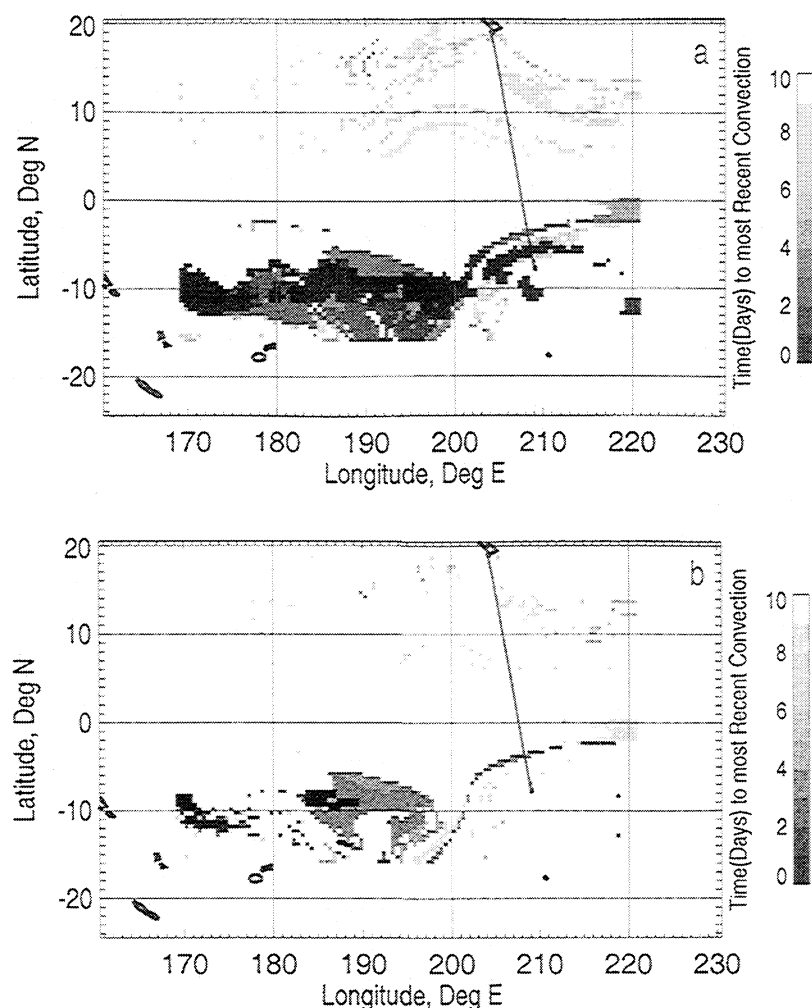


**Figure 5.** Gray scale coded times since the most recent encounter with convection of 10-day back trajectories originating in the west central Pacific region: (a) trajectories originate at flight time on 951220, assuming post-convective anvil heating as described in the text and (b) trajectories originate at flight time on 951220, assuming no postconvective anvil heating.

history of each parcel. Three points are to be noted. First the bulk of the trajectories come from the north and west. Some of these originate either in the Indonesian convective region or in the cold center near 150°E, 12°N (see Figure 1) and are effectively traveling around the monsoon anticyclone; others originate at the south edge of the subtropical jet. For all of the calculated trajectories, though, there is no evidence of any that came from a latitude greater than 35°N. Second, for three of the flights, 951215, 951220, and 960217, a significant number of trajectories from the south end of the flight track come from the general direction of the SPCZ. Third the temperature history for these two basic types of trajectories (from the north and west vs from the south) is distinctly different. For the northern trajectories, temperatures immediately prior to the time of observation were generally significantly warmer than at the time of observation, in some cases as much as 20 K warmer. For the southern trajectories, temperature

fluctuations during the 10-day history are much smaller (except for the strong penetrations into the southern summer midlatitudes in the flights of 951220 and 960217 depicted in Figures 4b and 4d). The implication is that the air in all the HACs on 951215 and 960213 and the northern HACs on 951220 has been too warm in the recent past to support clouds, implying fairly recent in situ formation.

Figures 5a and 5b shows the most important convective history parameter, namely the time since the most recent convection (if less than 10 days) experienced by a 1° by 1° grid of parcels at 1200 GMT on 951220. This was calculated by using the convective history method described in section 4 using 10-day back trajectories. For Figure 5a, postconvective anvil heating (section 4) was assumed, while for Figure 5b, no such anvil heating was assumed. As can be seen by the large areas in white, most of the parcels have not been influenced by convection in the most recent 10-day period, reflecting

the fact that the amount of area in the tropics occupied by thick anvils reaching the tropopause is fairly small. In fact, Figure 5a probably represents an upper limit, given the assumptions about the lapse rate described in section 4. For those parcels north of the equator that have been influenced by convection, the time since that occurred is consistently quite long, a week or more. This reflects the fact that this convection occurred in the Indonesian region, and a significant amount of time has elapsed as the parcels have traveled around the anticyclone. Times are shorter for parcels from the SPCZ region. Notably, however, these times are often still several days in length, although the shortest times (within the SPCZ itself) are well under a day. Though the assumptions for convective interaction between Figures 5a

and 5b are quite different, the basic picture of convective influence in the west central tropical Pacific is still qualitatively the same, with scattered convective influence north of the equator, and a fairly solid mass in the convective SPCZ region. Both figures have streamers of convective influence extending northeastward from the SPCZ, intersecting the flight track between  $3^{\circ}\text{S}$  and  $5^{\circ}\text{S}$ . Figure 5a shows two such streamers, the more northern one having been influenced by convection about 3–4 days previous, while the southern streamer has been influenced within the previous 12 hours. Figure 5b shows only the northern streamer intersecting the flight track at  $3^{\circ}\text{S}$ . The positional uncertainty in the trajectory calculations is probably too large to establish whether the cloud in Figure 2b between  $3^{\circ}\text{S}$  and  $7^{\circ}\text{S}$  is associated

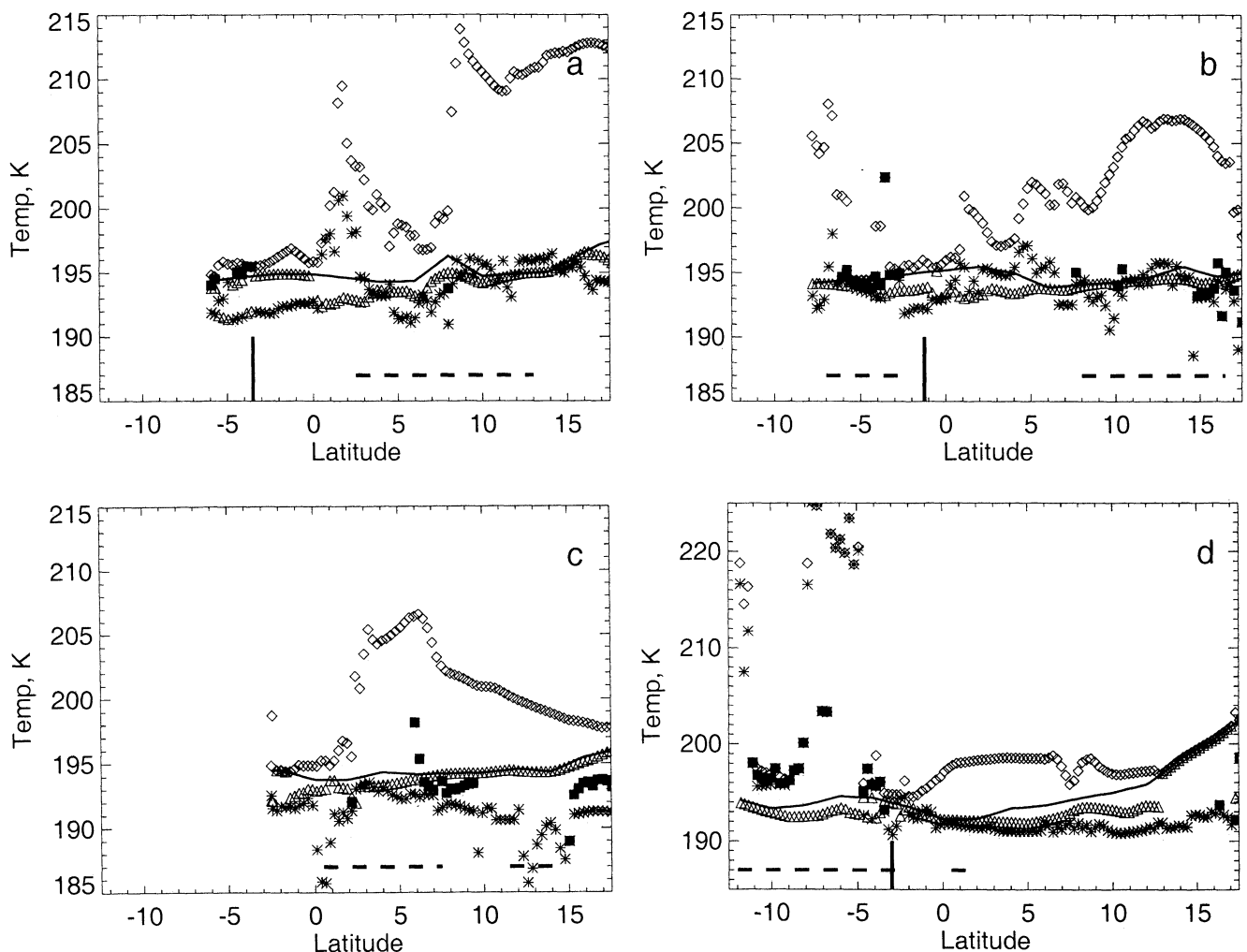


**Figure 6.** Summary thermal histories of back trajectories on the 380 K surface from points along the DC-8 flight track for the flights of (a) 951215, (b) 951220, (c) 960213, and (d) 960217. The solid line denotes the temperatures on the 380 K surface at the time of observation by the DC-8 along the flight track. The diamonds denote the warmest temperatures along the trajectory. The asterisks and triangles denote the coldest temperatures reached before and after the time of this “warm point,” respectively. For those parcels that have been convectively influenced in the past 10 days, the parcel temperatures at which that convective influence occurred are denoted by solid squares. For these convectively influenced parcels, only times after the time of convective influence are considered in evaluating the “warm point” and the two surrounding “cold points.”

with the “older” or “younger” streamer. The flight of 951220 had the largest differences in convective history between the anvil heating and no anvil heating calculations. For other flights where temperature and convective history indicated that the cirrus cloud was the remains of a convective anvil, anvil ages calculated by the two methods were similar.

Figures 6a–6d shows a summary of the temperature and convective history of the parcels along the flight track for each flight, plotted as a function of latitude (since all the flights were largely north–south). The demarcation between points whose back trajectories lead to the north and west and those whose back trajectories lead to the south is shown as a black slash on the axis, while the locations of observed HACs at 380 K is denoted by heavy horizontal black lines. Though HACs were observed on all flights, each flight does have a different pattern of the types of HACs and where they were observed. Thus we will discuss the temperature and convective history of the air parcels sampled by each flight in turn.

Perhaps the simplest flight to understand is that of 960217, where HAC2s at 380 K were confined to the region south of about  $2.5^{\circ}\text{S}$  (Figure 2e). This location corresponds roughly to the demarcation between southerly and northerly trajectories (Figure 4d) and the region of convective influence in the past 10 days. There are two regions of convective influence shown in Figure 6d, both south of  $3^{\circ}\text{S}$ . The northern one ( $3^{\circ}$ – $5^{\circ}\text{S}$ ) has a variety of convective sources with a minimum age of  $\sim 3$  days, and the southern one ( $7^{\circ}$ – $11^{\circ}\text{S}$ ) has a single source with an age of  $\sim 1.6$  days. In both cases, the source of convective influence is the SPCZ. Notably, the gap in convective influence at  $6^{\circ}\text{S}$  in Figure 6d coincides roughly with a minimum in the TSR at  $6^{\circ}$ – $7^{\circ}\text{S}$  between two maxima (Figure 2e). Figure 6d shows that in the southern area of convective influence, a gradual cooling followed the convective injection, with minimum temperatures only slightly below those at the time of observation reached 0.1–0.3 days before the time of observation. Given the uncertainties in the trajectories and the temperatures, one would conclude that the residual cloud has probably not evaporated during that last 0.1–0.3 days of slight warming. Just north of the southern convective influence region, Figure 6d indicates a sudden jump to very high maximum values in the temperature history. This is due to the midlatitude origin of these air masses, and their passage through the SPCZ region during periods when convective activity did not reach high enough altitudes. The absence of convective influence, however, does not imply that no cloud should be observed. In fact, throughout the  $5^{\circ}$ – $8^{\circ}\text{S}$  region, the temperature history indicates continual cooling with a minimum attained less than 0.5 days before the time of observation. Again, the presence of cloud is not inconsistent with this temperature history; the warming at the end of this history is too small and occurs over too short a time to argue conclusively that the cloud that may

have formed during the prolonged cooling has evaporated. The temperature history in the region between  $3^{\circ}\text{S}$  and  $5^{\circ}\text{S}$  is more variable, with convective influence from a variety of sources. The parcel most recently influenced by convection, however, is at  $\sim 4.5^{\circ}\text{S}$  (3 days). Following that injection it then cooled to  $\sim 192\text{ K}$   $\sim 1.2$  days prior to the time of observation, followed by warming to 196 K and subsequent cooling to 194 K. In fact, all the parcels in this  $3^{\circ}$ – $5^{\circ}\text{S}$  region underwent significant warming (2–3 K) over a greater than 1 day period prior to the time of observation. This suggests that a 2–3 K warming may be insufficient to evaporate all the ice crystals injected by the convection and condensed by the cooling following that convection.

The back trajectories for 960217 from locations north of  $2^{\circ}$ – $3^{\circ}\text{S}$  are all essentially from the north and west, passing at least partway around the monsoon anticyclone (Figure 4d). North of  $3^{\circ}\text{N}$ , the parcels have experienced temperatures at least 2 K colder than the current temperature more than a week prior to the time of observation. In fact, north of  $3^{\circ}\text{N}$  the coldest temperatures in the 380 K 10-day parcel histories are generally the coldest of all the four flights. North of  $6^{\circ}\text{N}$ , the 380 K temperatures at the time of observation on this flight are generally the warmest of all the four flights. Arguably, then, the cold temperatures in the parcel histories have “wrung out” significant amounts of water vapor through condensation and subsequent sedimentation. The cooling of the parcels as they move southward toward the equator in the eastern branch of the anticyclone is insufficient to form clouds. There is a region between  $3^{\circ}\text{S}$  and  $3^{\circ}\text{N}$  where the coldest temperatures are very close to the temperatures at the observation point. This is not inconsistent with the cloud observations, though, as there is some observed cloud at  $2^{\circ}\text{N}$  (Figure 2e).

The flight of 960213 (Figures 2c and 2d, Figure 4c, and Figure 6c) is a complete contrast to the 960217 flight in that it has only HAC1 type clouds. As Figure 4c shows, all the back trajectories are northerly, having traveled partway around the Northern Hemisphere anticyclone depicted in Figure 1b. As shown by the relatively large number of solid squares in the northern part of the flight track (Figure 6c), 380 K air on this flight is strongly influenced by convection, essentially because a relatively large proportion of the trajectories are from the western Pacific convective region (Figure 4c). However, as Figure 6c shows, all this convectively influenced air cools somewhat after the convection, as indicated by the asterisks in the figure. This would be expected to lead to further ice crystal growth, subsequent sedimentation, and consequent loss of water vapor. The air then warms by between 5 K and 15 K, presumably due to descent as it travels northward into the subtropical jet region prior to arriving in the area of observation. Any residual ice crystals from the convective outflow would thus almost certainly evaporate. Effectively, all the “memory” of the convective injection

tion temperatures has been “lost” as the parcels cool and warm following the convection. In fact, there is little apparent spatial relationship between the HACs and the region of convective influence. Overall, except for a region between  $3^{\circ}$ – $4^{\circ}$ N, the minimum parcel temperatures in the history are all substantially lower than the current temperatures. Arguably, then, one would not expect formation of clouds on a large scale and, indeed, we did not observe the extended continuous sheets seen by *Winker and Trepte* [1998]. Rather, one sees sloping structures that actually occupy a mesoscale region at any given altitude or potential temperature surface. Section 6 discusses how gravity and inertia-gravity waves might generate these structures.

The two February 1996 flights each contain one of the two HAC types, whereas the December 1995 flights have both cloud types. Turning first to 951220 (Figure 2b), we note an HAC2 cloud south of  $\sim 2.5^{\circ}$ S, and HAC1 between  $8^{\circ}$ N and  $16^{\circ}$ N. On the 380 K surface, the air parcels along the flight track have the same basic pattern of trajectory origins (Figure 4b) as for the 960217 flight, with air south of the equator having basically southerly trajectories, and air north of the equator, northerly. Convective influence within the past 10 days is strongest (in terms of proportion of parcels influenced) south of  $\sim 2.5^{\circ}$ S (Figure 5a), with two regions  $\sim 0.5$  days ( $6^{\circ}$ S to  $4.5^{\circ}$ S) and 3.5 days ( $\sim 3^{\circ}$ S) old. The temperature history for the southernmost of these two regions (Figure 6b) indicates roughly constant temperature between the convective injection and the time of observation, certainly consistent with the continued presence of cloud. For the region near  $3^{\circ}$ S, the air cools perhaps 2 K and then warms slightly for  $\sim 0.5$  days prior to observation. Though not as clear cut as for the southernmost region of convective influence, these temperature variations are not large enough (when uncertainty is taken into account) to rule out the possibility of convective outflow cloud. Notably there is no convective influence north of  $2.5^{\circ}$ S, which is the northern edge of the observed cloud in Figure 2b. This further reinforces the interpretation that the HAC2 cloud south of  $2.5^{\circ}$ S is a residual from convective outflow. Convective influence is also found north of  $\sim 7^{\circ}$ N. As for 960213, however, this convective injection has occurred between 7 and 10 days prior to the time of observation and is followed by the same substantial warming as the air parcels flow northward into the subtropical jet. Thus, as for 960213, the observed clouds between  $8^{\circ}$ – $16^{\circ}$ N are clearly not due to convective outflow. Unlike 960213, however, the coldest temperatures in the parcel history for much of the HAC1 region ( $10.5^{\circ}$ – $14^{\circ}$ N; Figure 6b) are quite close to the current temperatures, and these temperatures occur within 0.5 days of the time of observation. Thus, in this case, it is quite plausible that the large-scale cooling associated with the equatorward air motion could be responsible for much of the HAC1 between  $8^{\circ}$ – $16^{\circ}$ N. In fact, the larger extent of the cloud on the 380 K and 390 K potential temperature surfaces (about 600 km)

vis a vis the much narrower sloping clouds on 960213 is consistent with this scenario. The temperature history along other parts of the flight track that have no cloud is reasonably consistent with the cloud observations. Between  $2.5^{\circ}$ S (the northern edge of the observed cloud) and  $\sim 4^{\circ}$ N the parcels experienced significantly colder than current temperatures between 1 and 7 days prior to the time of observation. The implication is that water vapor has been removed from the air parcels by condensation due to cold temperatures. Subsequent warming of 3–4 K would then evaporate any remaining ice crystals.

The flight of 951215 (Figure 6a) is the most ambiguous of the four in that this is the only case where HAC2s are found in the northern portion of the flight track. As in the previous flights, parcels at the southern end (south of  $\sim 3^{\circ}$ S in this case) have sufficient southerly trajectories to reach the mean position of the SPCZ (Figure 4a). There are regions south of  $3^{\circ}$ S where convection has influenced the air parcels within the past 5–7 days. Unlike 960217 and 951220, however, where HAC2s were observed in these convectively influenced regions, there is no evidence of cloud south of  $3^{\circ}$ N. This absence of cloud is consistent with the temperature history, which shows cooling following the convective injection to temperatures 3–4 K below the temperature at the time of observation. These minimum temperatures occurred 2 days prior to the time of observation. These cold temperatures may well have removed water vapor above the saturation mixing ratio. The air subsequently warmed by 3–4 K until the time of observation; this warming presumably evaporated any left over ice crystals. North of  $3^{\circ}$ S, convective influence is very minimal. Moreover, the temperature histories indicate very little potential for large-scale cloud formation along the flight track between  $3^{\circ}$ S and  $8^{\circ}$ N. This is because there is significant warming of 3–4 K in the 2–5 days prior to the time of observation. As suggested above, the earlier cold temperatures would arguably remove sufficient water vapor to make the air too dry to condense at temperatures at the observation time. However, there is, in fact, a quite thick HAC2 between  $4^{\circ}$ – $7.5^{\circ}$ N, entirely inconsistent with these expectations. There is also significant cloud north of  $8^{\circ}$ N, both of the thick HAC2 variety and the thinner, sloping HAC1 (Figure 2a). In contrast to the region between  $4^{\circ}$  and  $7.5^{\circ}$ N, temperatures at the observation time between  $8^{\circ}$  and  $15^{\circ}$ N are actually quite close to the coldest in the entire parcel history, indicating that this region does have the potential for producing cloud. The flight of 951215 differs from the other three in one important respect, which may account for the thick clouds observed between  $4^{\circ}$  and  $12^{\circ}$ N. The northern ITCZ at around  $8^{\circ}$ – $10^{\circ}$ N, west of the flight track was unusually active. This has no direct impact in terms of convective blowoff, since tropopause winds are westward, away from the flight region. However, these convective systems may generate high-amplitude gravity waves that produce significant mesoscale tem-

perature variations, temperature variations that might account for the observed HAC2s.

In summary, the four case studies show that the presence or absence of HACs, and their morphology, is at least qualitatively consistent with the convective and temperature history of the air parcels. For the portions of the flight tracks where the air parcels had northerly back trajectories, convective injection, if any, occurred on the order of a week prior to the observation time. This convective injection was usually followed by (1) further cooling of a few degrees, (2) significant warming to temperatures 5–10 K or more above those at the time of observation, and (3) cooling to the current temperature. The major implication is that any convective blowoff in this northerly back trajectory region has almost certainly evaporated prior to the observation time. Thus clouds in this region are condensed from clear air and, except for 951215, are thin, sloping structures with a low TSR (HAC1). The extent of these clouds is for the most part consistent with the temperature history. In other words, it is qualitatively consistent with the notion that cold temperatures earlier in a parcel's history can condense and remove sufficient moisture so that temperatures must get at least as cold again to form cloud. When the temperatures at the time of observation are close to the coldest in the air parcel history (951220 and 951215), cloud coverage is fairly extensive. Otherwise, there is either no (960217) or very limited (960213) coverage. Where cloud is observed in contradiction to the temperature history, there is either limited indirect evidence (951215) or very direct evidence (960213, see section 6 below) for mesoscale motions on the scale of the observed HACs.

Those portions of the flight tracks where the air parcels had a southerly back trajectory always had significant, fairly recent convective influence from the SPCZ. Three of the flights (951215, 951220, and 960217) had such convective influence, and in two cases, fairly thick HAC2s were observed. It is likely that these clouds were residual ice crystals from convective blowoff, that is, anvils that had been able to maintain themselves because of either slow cooling or only minimal warming. No cloud was observed in the southerly trajectory portion of the 951215 flight, due to significant warming between the time of convective injection and the observation time. If these clouds are indeed convective blowoff, it implies a significant lifetime for some of these anvils, ranging from 0.5 days (951220) to 3 days (960217) in the cases considered here. Such long lifetimes are implied by the recent work of Sherwood [1999], who has shown that the formation and radiative rise of convective anvils essentially advects the mean moisture gradient upward. This advection supplies moisture to the tropopause region and, in the absence of significant synoptically imposed downward motion, can allow a thin cirrus cloud to maintain itself. It should be noted that due to sedimentation, the ice particles in the HAC are unlikely to be the same ones that were present right

after convection occurred. Thus a "3 day lifetime" for an outflow cirrus cloud really means that the relevant air parcel has been occupied by cloud continuously since the formation of an anvil by convection.

Two shortcomings of the GEOS-1 analyses and their impact on these conclusions require some discussion: (1) the GEOS-1 analyses overestimate the tropopause temperature by  $\sim 3$  K and (2) these analyses fail to include significant mesoscale temperature fluctuations. This is evident from MTP measurements (Figure 2) and from explicit comparisons with in situ aircraft data. The impact of these limitations of the analyses on our conclusions are probably small. First the overestimate of tropopause temperatures appears to be due to the "rounding" of the sharp tropical tropopause by the limited (1 km) vertical resolution of the analyses. Since most of the trajectories are confined to the tropical regions, with similar tropopause "sharpness," the temperature error is probably systematic. Since the conclusions of the trajectory analyses are based on comparative rather than absolute temperatures, a largely systematic error should not impact them. Mesoscale temperature fluctuations are clearly important, and, for sufficiently long timescales, Jensen *et al.* [1996] have shown a significant impact on water vapor content. However, Jensen *et al.* [1996] also show that the shortest scales may have very little impact because the very rapid cooling rates produce large numbers of small particles. These are not able to sediment prior to the air parcel returning to equilibrium, reheating, and reevaporating the small particles.

The quality of the trajectory analyses and temperature histories, as manifested by the correct positioning of the convectively influenced air from the SPCZ (and HAC2s), implies that the GEOS-1 analysis winds in the tropopause region must be quite good. This issue can be further examined by comparing in situ winds measured by the two aircraft used in this study, the DC-8 and the ER-2 (see section 6) with GEOS-1 analyses. DC-8 and ER-2 measurements are made at  $\sim 200$  and  $\sim 50$  mb, respectively, so neither is exactly at the altitude of interest ( $\sim 100$  mb). The comparisons (not shown) indicate good agreement between the wind analyses and measurements at DC-8 levels (for the four flights of interest) and poor agreement at ER-2 levels (for the one flight where ER-2 data was available, 960213). The basic interpretation is that the GEOS-1 analyses faithfully render the large- and synoptic-scale circulation in the tropics, which, in this case, extends up to  $\sim 100$ –80 mb (Figure 1). This circulation becomes much weaker at ER-2 altitudes, where wind variations are dominated by smaller-scale gravity waves (see section 6).

## 6. Generation of High Altitude Cirrus by Gravity Waves: A Case Study

The flight of 960213 is unique in two ways. First, both the narrow mesoscale extent of the clouds and the

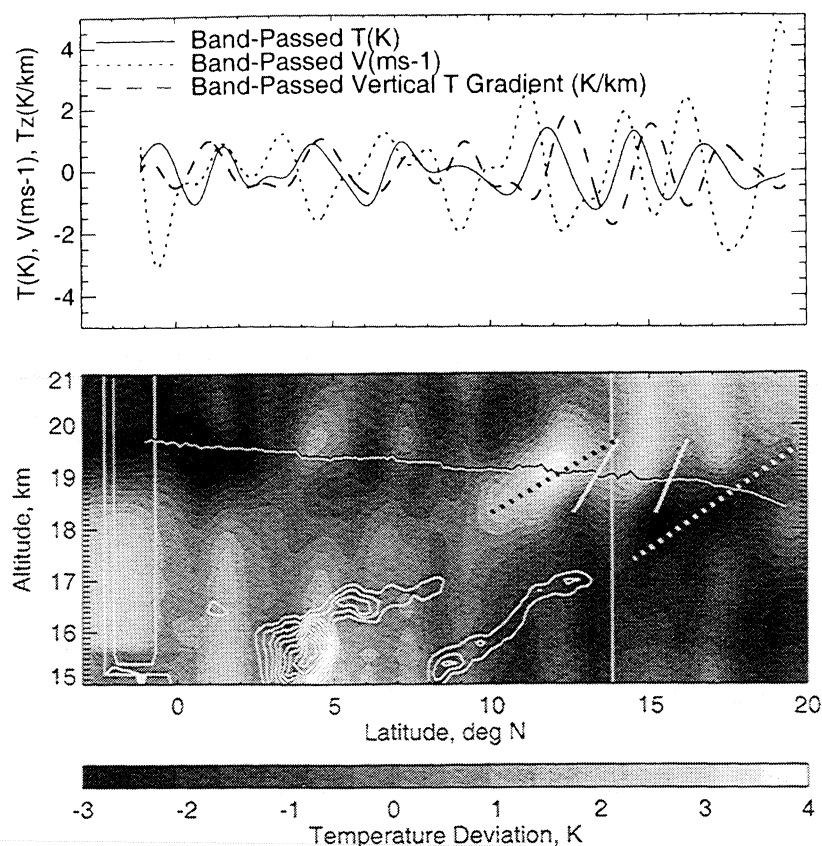


**Figure 7.** (bottom) Contours of  $\log(\text{TSR})$  at intervals of 0.05 for the southbound leg of the DC-8 flight of 960213 (white contours) superimposed on ER-2 MTP temperature deviations from the horizontal average for the southbound leg of the ER-2 flight of 960213. The ER-2 flight track is shown by the black and white line. (top) Band-pass filtered meteorological variables from southbound leg of the ER-2 flight of 960213. See text for further details.

temperature history indicate that mesoscale temperature or water vapor fluctuations are responsible for the clouds. Second, an ER-2 flight of similar length to the DC-8 flight occurred along the same horizontal path. This flight was centered in time  $\sim 16$  hours after the midpoint of the DC-8 flight. Hence, in situ sampling was available where the large-scale conditions (if not the mesoscale conditions) were very similar to those during the DC-8 flight. Presumably, the character of the mesoscale motions during the two flights, if not the exact placement, would be similar.

The ER-2 flew directly south to  $\sim 1^\circ\text{S}$  on the  $155^\circ\text{W}$  meridian at  $\sim 19$  km. Upon reaching  $1^\circ\text{S}$ , the aircraft turned around and descended to 15.5 km, ascending immediately thereafter, thus providing two vertical profiles spanning  $\sim 4^\circ$  of latitude around the equator. With the exception of the profiles at the equator, the altitude of the ER-2 measurements is significantly higher than the region of HACs near the tropopause. However, since the vertical stratification at ER-2 altitudes is comparable to that in the tropopause region, we expect the nature of the mesoscale motions at the tropopause (e.g., gravity waves) to be more nearly similar to the

mesoscale motions at ER-2 altitudes than those at DC-8 altitudes, where the atmosphere is close to adiabatic. The available relevant ER-2 measurements were in situ temperature, pressure, and winds (Meteorological Measurement System (MMS)) [Gaines *et al.*, 1992], vertical temperature profiles in an 8 km deep curtain centered at the aircraft altitude (Microwave Temperature Profiler (MTP)) [Gary, 1989], and water vapor from a Lyman- $\alpha$  hygrometer [Hintsa *et al.*, 1998]. The critical questions are (1) is there evidence of mesoscale temperature fluctuations with a structure resembling that of the observed HACs, (2) what is the mechanism responsible for these fluctuations, and (3) is there evidence of water vapor at or near saturation in the in situ measurements near the tropopause?

Figure 7 (bottom) shows a latitude-height curtain of the deviation of temperature from its horizontal average, as measured by the ER-2 MTP. The data have been low-pass filtered so as to remove all variance with wavelengths shorter than 180 km. On this are superimposed the southbound DC-8 TSRs taken  $\sim 16$  hours before the ER-2 curtain. Note that the MTP provides its highest vertical resolution near the ER-2 aircraft alti-

**Table 2.** Properties of the gravity waves shown in Figures 7-9

| Wave            | $\delta T$ | $\delta V $ | $N \delta Z $ | $\lambda_v$ | $\lambda_h$ | $c_d$ | Period | $c_{gv}$ | $c_{gh}$ |
|-----------------|------------|-------------|---------------|-------------|-------------|-------|--------|----------|----------|
| Short wave      |            |             |               |             |             |       |        |          |          |
| ER-2 horizontal | 2.6        | 4.0         | 4.4           | 5.0         | 280         | 20.0  | 4      | .38      | 17       |
| Long wave       |            |             |               |             |             |       |        |          |          |
| ER-2 horizontal | 4.8        | 9.0         | 8.3           | 3.0         | 1100        | 13.5  | 23     | .04      | 10       |
| “Cloud” wave    |            |             |               |             |             |       |        |          |          |
| DC-8            | ?          | ?           | ?             | 1.0         | 550         | 3.8   | 40     | .0065    | 1        |
| Equatorial wave |            |             |               |             |             |       |        |          |          |
| ER-2 Vertical   | 5.0        | 9.3         | 8.7           | 1.3         | ?           | 5.3   | ?      | ?        | ?        |

From left to right: Peak-to-peak temperature variation (K); peak-to-peak wind variation ( $\text{m s}^{-1}$ ); peak-to-peak variation in the product of the Brunt-Vaisala frequency and the vertical displacement ( $\text{m s}^{-1}$ ); vertical wavelength (km); horizontal wavelength (km); Doppler-shifted (intrinsic) phase speed ( $\text{m s}^{-1}$ ); intrinsic period (hours); vertical group velocity ( $\text{m s}^{-1}$ ); and horizontal group velocity ( $\text{m s}^{-1}$ ).

tude; thus the “die-off” of short vertical-scale phenomena away from the aircraft is an instrumental effect. Between  $\sim 10^\circ$ – $18^\circ\text{N}$  at  $\sim 19$  km there are upward and northward sloping structures, highlighted by two sets of overplotted sloping lines. The solid white lines highlight the negative temperature perturbations of a wave with a wavelength of  $\sim 2.5^\circ$ , while the white and black dotted lines highlight the negative and positive perturbations respectively of a longer, shallower phenomenon. Slopes in the temperature perturbations are hallmarks of atmospheric internal gravity waves [Holton, 1972, pp. 172–176], though this does not by itself prove that the phenomena are gravity waves. To do that one must examine the other meteorological variables (e.g., horizontal winds), analyze their amplitude and phase relationships, and compare those relationships with theory. This is done in Figure 7 (top), which shows the in situ ER-2 meteorological variables, band-pass filtered (to include wavelengths between 180 and 500 km) to show only variance with the characteristic horizontal wavelength of the shorter,  $2.5^\circ$  structures highlighted by the solid white lines. Of interest are the two temperature “valleys” at  $13.3^\circ\text{N}$  and  $15.7^\circ\text{N}$ , which coincide with the sloping structures highlighted by the white solid lines in Figure 7 (bottom).

The gravity wave properties based on the observed meteorological variables in the  $11^\circ$ – $18^\circ\text{N}$  region depicted in Figure 7 (top), and summarized in the first line of Table 2, clearly show that the temperature structures are northward and upward propagating gravity waves. This is demonstrated in three ways. First, the quadrature ( $90^\circ$  out of phase) relationship between  $T$  and  $V$  is consistent with that expected for gravity waves. Second, hydrostatic gravity waves in a slowly varying environment exhibit a “universal” relationship between the temperature and horizontal wind perturbations described as

$$\delta|V| = N\delta|Z|, \quad (1)$$

where  $\delta|Z|$  is the vertical displacement, uniquely related to the temperature perturbation, and  $N$  is the buoy-

ancy frequency. As the first line of Table 2 shows, the observed meridional wind perturbation is very close to that derived from the temperature perturbation. Third, Figure 7 (top) shows that  $V$  and  $T_z$  (the vertical temperature gradient) are negatively correlated; this, along with the slope of the structures, indicates that the phase propagation is downward and northward with respect to the flow, an indicator of upward and northward group velocity. The zonal wind perturbation (not shown) is smaller than the meridional wind perturbation and lacks any coherence with  $T$ , thus showing that this wave has only a small zonal component to the horizontal wavenumber vector. However, it is clear from Figure 7 that these gravity waves are not a candidate for explaining the observed HAC1s; the upward and northward slope of the gravity waves is obviously too steep. Also, that slope is unlikely to have been significantly less steep at the lower altitudes from which the waves have propagated, since the meridional wind and stability that govern the vertical wavelength are substantially the same near the tropopause.

However, there is evidence for shallower sloping structures, as suggested by the temperature perturbations highlighted by the dotted lines in Figure 7 (bottom). Figure 8 uses the same data as Figure 7, except that all variables (except for the TSR in Figure 7 (bottom)) are low-pass filtered to exclude the wavelengths depicted in Figure 7 (means and trends have been removed as well). The sloping dotted lines are positioned as in Figure 7. At these scales, we also see an upward and northward slope, except with a much shallower slope than for the shorter waves. As before, there is a clear quadrature ( $90^\circ$  phase) relationship between  $V$  and  $T$  that suggests that the sloping structure is a gravity wave and an amplitude relationship between  $V$  and  $N\delta|Z|$  that confirms it (second line of Table 2). Again, the zonal wind variance (not shown) is not coherent with the meridional wind. The inferred (from the vertical wavelength) Doppler shifted frequency is 3 times the Coriolis parameter, which means that this wave, like the shorter one, is most likely a pure, hydrostatic, planar gravity

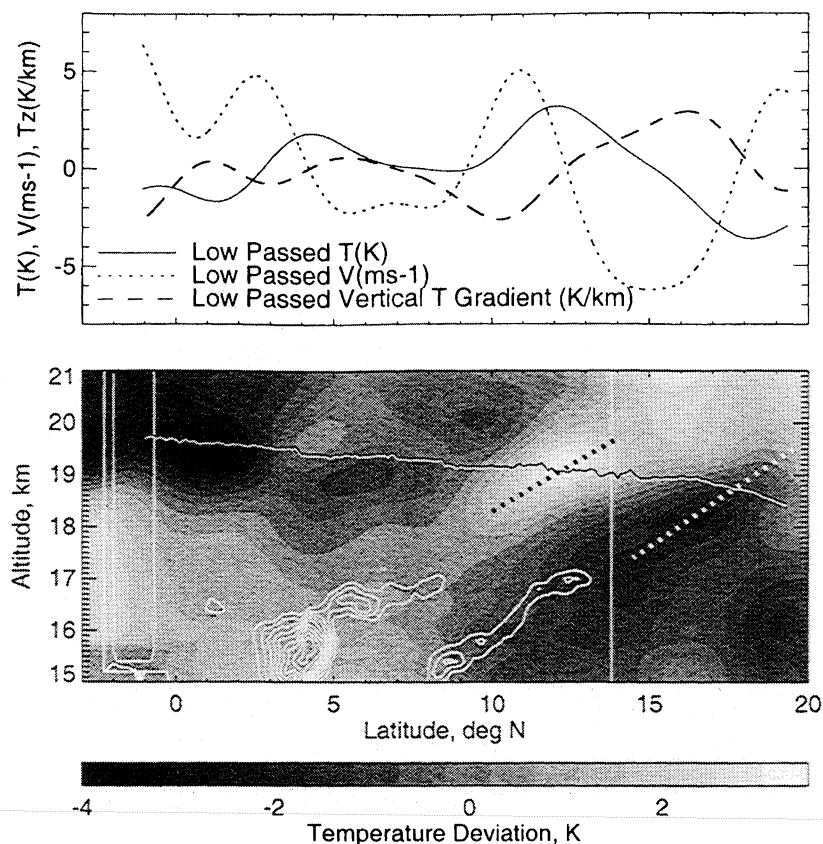


**Figure 8.** (bottom) As in Figure 7(bottom), except that the ER-2 MTP temperature deviations are low-pass filtered to remove all wavelengths less than 500 km. (top) Low-pass filtered meteorological variables from the southbound leg of the ER-2 flight of 960213. See text for further details.

wave. This wave, or one like it, is a more likely candidate for explaining the sloping HACs between  $3^{\circ}$ – $14^{\circ}$ N, though the wave slope (or ratio of horizontal to vertical wavenumbers) is  $\sim 1.5$  times that of the slope of the HACs (compare third line of Table 2).

Nevertheless, gravity waves with slopes and horizontal wavelengths roughly comparable to those of the clouds are clearly present within 10–20 hours of the cloud observations. Moreover, those gravity waves are propagating upward, indicating that they have been at the tropopause at one time even though they are observed at 19 km. Their temperature amplitudes are substantial, 1.3 K for the short waves and 2.4 K for the long waves, implying saturation mixing ratio changes of 0.9 ppmv and 1.8 ppmv, respectively, from the background. The implication is that mesoscale gravity waves alone are capable of producing subvisible cirrus clouds at the tropopause. Thus, as *Jensen et al.* [1996] and *Potter and Holton* [1995] indicate, these motions could well play a role in dehydrating the air in the tropopause region prior to its entry into the stratosphere. Another key parameter is the intrinsic period of the gravity waves (the period as seen by an air parcel flowing through the waves). This is important because it governs the cooling rate experienced by the air and hence

the size of the ice crystals that could be formed [*Jensen et al.*, 1996]. The periods of the three different waves illustrated in Figures 7 and 8 (including the “wave” determined by the cloud structure, third line of Table 2) vary from 4 to  $\sim 40$  hours. On the basis of *Jensen et al.*’s [1996] work, the two longer period waves would certainly imply cooling rates that are sufficiently slow to produce large enough ice crystals for fallout and dehydration in the timescale of the wave.

Further evidence that gravity waves could produce HACs is shown in Figures 9a and 9b. These are vertical profiles, with the descent (Figure 9a) extending from  $1^{\circ}$ S to  $0.5^{\circ}$ N while the ascent (Figure 9b) extends from  $0.5^{\circ}$ N to  $3^{\circ}$ N. These profiles are well south of the upward and northward sloping HACs between  $4^{\circ}$ S and  $13^{\circ}$ N discussed above, so they do not provide a direct explanation of those phenomena. However, the profiles can unambiguously define the height of the tropopause and provide information about possible other gravity waves close to the equator. The key feature of these profiles is that both are saturated near the tropopause, with the descent saturated from 16 to 16.7 km and the slightly colder ascent from 15.75 to 16.9 km. Though there was no instrumentation on the ER-2 for detecting cloud particles, pilot reports indicate very thin cirrus

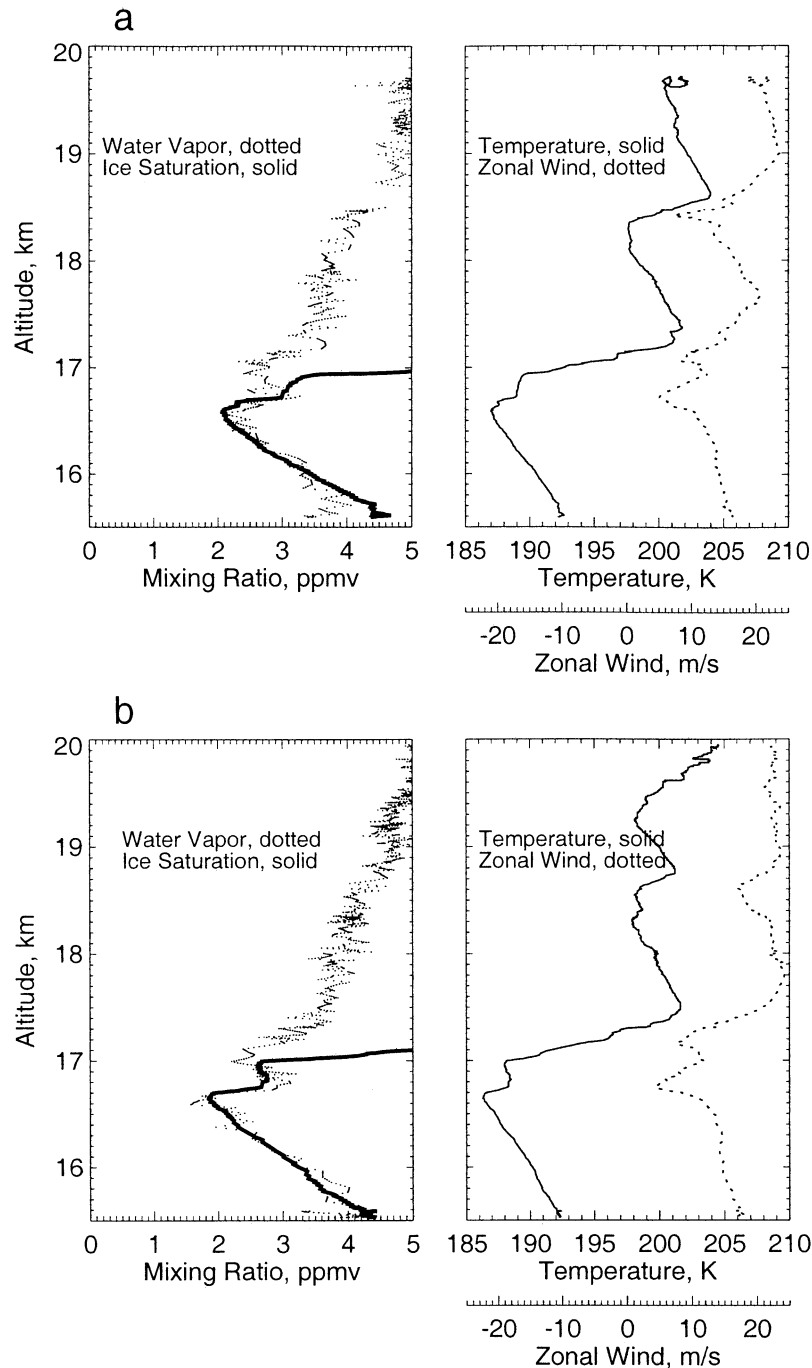


**Figure 9.** In situ water vapor, ice saturation mixing ratio, zonal wind, and temperature from the ER-2 descent and ascent near the equator on the flight of 960213. (a) Data from descent centered at  $\sim 0.4^\circ\text{S}$ ; (b) data from subsequent ascent centered at  $\sim 1.5^\circ\text{N}$ .

below the aircraft at  $1.5^\circ\text{N}$ , clearly consistent with the observations of saturation. (*Tuck et al.* [1997] has also reported a case in October of 1994 where there is clear in situ evidence from particle data of thin cirrus at the tropical tropopause in the mid-Pacific.) The highest altitude of saturation is actually roughly consistent with the top of the HAC1 in Figure 2d at the lowest latitudes ( $\sim 2^\circ\text{N}$ ). A small region above the tropopause at 16.65 km ( $\sim 370\text{ K}$ ) in Figure 9b is clearly saturated, and

this tropopause is actually fairly close to the top of the “blob-like” structure in Figure 2c at  $3^\circ\text{--}5^\circ\text{N}$ . Thus if we assume that the tropopause in Figure 9 also applies to Figures 2c and 2d, we could tentatively conclude that the sloping portions of the HAC1s in Figures 2c and 2d between  $3^\circ\text{N}$  and  $8^\circ\text{N}$  are actually just above the tropopause, with the blob-like structure below it.

The role of gravity waves is illustrated by comparing the vertical profiles of temperature and zonal wind in

Figures 9a and 9b. There is a clear quadrature relationship in the vertical between these two meteorological quantities in the 16.5–19.5 km region, with a vertical wavelength of  $\sim 1.3$  km. Also, as the fourth line of Table 2 shows, the quantitative relationship between the wind perturbation and  $N\delta|Z|$  holds reasonably well. There is little coherence with the meridional wind, so this wave appears to be propagating roughly east–west. If an upward group velocity is assumed, the observations imply an eastward propagating gravity wave with a Doppler-shifted phase speed of  $\sim 5$  m s $^{-1}$ . Notably, this is comparable to the zonal wind amplitude of the wave, so the wave is actually quite close to breaking. At the tropopause, the wave’s temperature perturbation will manifest itself partly as a rise and fall of the tropopause, resulting in a peak-to-peak variation of  $\sim 5$  K in the tropopause temperature (based on the temperature amplitude exhibited by the wave in the stratosphere). This implies a 2.5 ppmv peak-to-peak variation in saturation mixing ratio. It should be emphasized that the horizontal component of the aircraft’s flight track is along (rather than perpendicular to) the wave’s phase surfaces (the wave is propagating eastward while the aircraft is moving northward). Thus the observed temperature differences between the two profiles at the tropopause due to the wave will be relatively small. These differences will be more a manifestation of latitudinal amplitude variation than of phase variation.

The questions of how and where the observed gravity waves are generated is important, since the answers to those questions will indicate how representative these observations are of the tropics as a whole. For the waves observed on the level leg of the ER-2 flight, as well as those presumed responsible for the HAC1s observed by the DC-8 (first three lines of Table 2), we can calculate vertical and horizontal group velocities. The important point about these group velocities is that a crude backward trace to the tropopause level indicates a “point of origin” no further south than the equator. It is thus doubtful that these particular waves have their source at the SPCZ at 10°S to 15°S. It is more likely that they are produced by imbalances in the flow caused by the upper tropospheric trough “digging” south toward the equator. That imbalances in the flow can produce gravity waves has been demonstrated by the modeling work of *O’Sullivan and Dunkerton* [1995]. In their work, baroclinic development at midlatitudes produced inertia-modified gravity waves. At these latitudes, however, the coriolis parameter is sufficiently small that waves with similar frequencies are not substantially modified by the Earth’s rotation. If this imbalance in the flow is indeed the mechanism for generating these waves, one cannot conclude that similar waves are necessarily found at other longitudes (though there is strong evidence for inertia-gravity waves throughout the tropics [*Karoly*, 1996]). In particular, the very cold region near 130°–175°E and 10°N (Figures 1a and 1b) does not typically experience strong digging troughs since it

is “protected” by a strong and steady subtropical jet to the north.

The waves observed during the ER-2’s dive at the equator may well have a different origin, though the absence of horizontal wavelength information limits the conclusions that can be drawn. The east–west propagation at least suggests the possibility that equatorially trapped modes [*Holton*, 1975, pp. 53–70] may play a role. If we assume that they are indeed equatorially trapped, forced gravity waves with a horizontal wavelength of less than 1500 km, the dispersion relationship is essentially that of a pure gravity wave, with the latitudinal trapping proportional only to the vertical wavelength and the Doppler-shifted phase speed. Applying the relevant equations, these assumptions imply an equatorial trapping distance of  $\sim 5^\circ$  of latitude. Because of the equatorial trapping and the implied confinement of wave energy, a very substantial horizontal propagation distance is possible for these waves, suggesting that they may have been generated by convection in the western Pacific. The DC8 TSR data actually give an indication that there is longitudinal phase variation in the temperature, since the northbound leg at (Figure 2d) has significantly more cloud near the equator than the southbound leg and that leg is  $\sim 2.5^\circ$  (275 km) further east.

## 7. Summary

This study has attempted to explain a given set of observations of thin cirrus clouds near the tropical tropopause with a view toward establishing their consistency with temperature and convective history and our limited understanding of their formation mechanisms. It represents a complementary approach to that of *Newell et al.*, [1996], who compared DIAL observations of tropical cirrus clouds near the tropopause with analyzed vertical motion and relative humidity fields. The basic structures and nature of the clouds found during the TOTE/VOTE experiment were similar to the findings of the space-based LITE experiment [*Winker and Trepte*, 1998]. Two basic types of clouds were found, extended laminar structures with horizontal extents up to 1000 km (HAC1, similar to those shown in *Winker and Trepte* [1998, Plate 1]) and blobbier, thicker structures resembling convective clouds (HAC2, similar to those shown in *Winker and Trepte* [1998, Plate 3]). Altitudes of these clouds were comparable to those in *Winker and Trepte* [1998], though the apparent convective outflows (HAC2) were higher. The latter is to be expected, since the tropopause height in the tropical central Pacific in Northern Hemisphere winter is generally higher than the tropopause height in September (the time of *Winker and Trepte*’s [1998] LITE observations). Comparing the TOTE/VOTE results with cirrus clouds observed during PEM-WEST by *Newell et al.* [1996], it appears that *Newell*’s clouds most strongly resembled the HAC2’s in this study.

For the most part, the positions of the respective cloud types were consistent with their convective and temperature histories. The HAC2s (except for the 951215 case) were found in the southern portions of the Hawaii-equator flight track and were consistent with convective outflow from the Southern Pacific Convergent Zone near  $10^{\circ}$ – $15^{\circ}$ S. In other words, back trajectories indicated encounters with significant convection in the previous 10 days, and the temperature histories indicated that the air had either cooled since the convective encounter or not warmed substantially. In one case where air had interacted with the SPCZ but no cloud was observed, the temperature history indicated substantial cooling after the convective encounter, followed by warming. Thus the absence of cloud was entirely consistent with the temperature and convective history. For the observed convective outflow clouds, the time since the most recent convection ranged from 0.5 days to 3 days. This is an important finding, since it suggests that convective outflow cirrus are not necessarily dissipated rapidly but can remain in the tropopause region for extended periods of time. This increases their potential for impacting the radiation budget [Jensen *et al.*, 1996]. The implication of this finding in the context of the recent work of Sherwood [1999] is that convective outflow can continue to rise and advect moisture into the tropopause region long after the convection has occurred. It also has potential importance to the dehydration issue. If the high supersaturation requirements (160%) for in situ ice nucleation of sulfate aerosols turn out to be a major barrier for the formation of in situ thin cirrus clouds at the tropopause [Koop *et al.*, 1998], then the ability of convective outflow cirrus (where ice crystals are already present) to act as “seeds” for the continued formation and growth of ice crystals may be very significant. In this context, Kelly *et al.* [1993] showed that cloud edges in the tropopause region over northern Australia during the convectively active monsoon coincided very well with 100% ice saturation.

In the northern portion of the flight track, the thin laminar cirrus structures tended to dominate. Again, their presence or absence, as well as their structure, was for the most part consistent with temperature and convective histories. Air north of the equator (approximately) had its origin either in the Northern Hemisphere subtropical jet or in the convective regions of the western equatorial Pacific and the equatorial Indian ocean. In any case, all the air passed through or near the subtropical jet. Thus it experienced temperatures upwards of 10 K warmer prior to being advected southward around the monsoon anticyclone (Figures 1a and 1b). The implication is that all the clouds were formed in situ, as any convective outflow would have evaporated prior to the time of observation. The structure and presence of the clouds were entirely consistent with temperature histories, with large-scale thin cirrus observed only on the flight where temperatures at the observation time were close to the coldest observed in

the entire temperature history. The one time where clouds were observed in spite of the relatively warm synoptic-scale temperatures, the clouds were strongly sloping and were actually quite limited in scale at any given altitude. The cloud structures resembled upward and northward propagating gravity waves, and such gravity waves were in fact observed  $\sim 16$  hours later at somewhat higher altitude with in situ ER-2 observations. The properties of these gravity waves indicated that they were potentially significant for dehydration, both from the point of view of the measured temperature perturbations and cooling rates. The temperature variations were several degrees peak-to-peak, implying a more than 2 ppmv variation in the saturation mixing ratio; this, in turn is  $\sim 70\%$  of the typical value of the water vapor mixing ratio at the tropopause in northern hemisphere winter. The wave periods, varying from 4 to 40 hours for cases isolated by the analysis, are long enough to allow large (10 microns or more) ice particles to form and fall out, thus effectively dehydrating the tropopause region [Jensen *et al.*, 1996]. If these waves are widespread in the tropics (and observations [e.g., Karoly *et al.*, 1996] indicate that they are) the implication is that they could effectively “ratchet down” the water vapor content in the tropopause region to values below those implied by synoptic-scale analyses at the tropopause or, for that matter, averages of tropopause cold point saturation mixing ratios from radiosondes [Dessler, 1998]. In fact, this gravity wave mechanism may not work as well as Jensen *et al.* [1996] suggest. In particular, ice supersaturations of as much as 160% may be required in order for sulfate particles (which predominate near the tropical tropopause) to freeze and begin the formation of ice crystals [Koop *et al.*, 1998]. In this case, gravity waves will only be able to “ratchet down” the water vapor content to 160% of the minimum ice saturation mixing ratio [Jensen *et al.*, 2000]. This ice supersaturation constraint may not apply, since Murphy *et al.* [1998] have shown that the composition of aerosols near the tropopause includes constituents other than sulfate, constituents whose nucleation properties are currently unknown. Another possibility is that we have not considered that each air parcel experiences not just the single, long-period gravity waves we have isolated in Table 1 but the complete spectrum. Thus, even though the temperature perturbation in the ER-2 flight leg is dominated by the 1100 km wave (see Table 1), the cooling rate associated with the 4 hour wave is actually larger by a factor of 3 (one sixth the period, half the amplitude). A complete assessment of how or even whether [Jensen *et al.*’s 1996] mechanism actually dehydrates air in the upper troposphere and lower stratosphere requires consideration of the entire spectrum of gravity waves, including some appropriate spectral model [Bacmeister *et al.*, 1996].

**Acknowledgment.** This work was funded by NASA’s Upper Atmosphere Research Program.

## References

- Ackerman, T. P., K. N. Liou, F. P. J. Valero, and L. Pfister, Heating rates in tropical anvils, *J. Atmos. Sci.*, **45**, 1606-1623, 1988.
- Allam, R. J., and A. F. Tuck, Transport of water vapour in a stratosphere-troposphere general circulation model I: Trajectories, *Q. J. R. Meteorol. Soc.*, **110**, 357-392, 1984.
- Bacmeister, J. T., S. D. Eckermann, P. A. Newman, L. Lait, K. R. Chan, M. Loewenstein, M. H. Proffitt, and B. L. Gary, Stratosphere horizontal wavenumber spectra of winds, potential temperature, and atmospheric tracers observed by high altitude aircraft, *J. Geophys. Res.*, **101**, 9441-9470, 1996.
- Browell, E. V., A. Carter, S. Shipley, R. Allen, and C. Butler, NASA Multipurpose Airborne DIAL System and Measurements of Ozone and Aerosol Profiles, *Appl. Opt.*, **22**, 522-534, 1983.
- Browell, E. V., S. Ismail, and W. V. Grant, Differential Absorption Lidar (DIAL) measurements from air and space, *Appl. Phys. B*, **67**, 399-410, 1998.
- Danielsen, E. F., In situ evidence of rapid, vertical, irreversible transport of lower tropospheric air into the lower tropical stratosphere by convective cloud turrets and by larger-scale upwelling in tropical cyclones, *J. Geophys. Res.*, **98**, 8665-8681, 1993.
- Denning, R. F., S. L. Guidero, G. S. Parks, and B. L. Gary, Instrument description of the airborne Microwave Temperature Profiler, *J. Geophys. Res.*, **94**, 16,757-16,765, 1989.
- Dessler, A., A Re-examination of the stratospheric fountain hypothesis, *Geophys. Res. Lett.*, **25**, 4165-4168, 1998.
- Gaines, S. E., S. W. Bowen, R. S. Hipskind, T. P. Bui, and K. R. Chan, Comparisons of the NASA ER-2 Meteorological Measurement System with radar tracking and radiosonde data, *J. Atmos. Oceanic Technol.*, **9**, 210-225, 1992.
- Gary, B., Observational results using the Microwave Temperature Profiler during the Airborne Antarctic Ozone Experiment, *J. Geophys. Res.*, **94**, 11,223-11,231, 1989.
- Hints, E. J., et al, Troposphere-to-stratosphere transport in the lowermost stratosphere from measurements of H<sub>2</sub>O, CO<sub>2</sub>, N<sub>2</sub>O, and O<sub>3</sub>, *Geophys. Res. Lett.*, **25**, 2655-2658, 1998.
- Holton, J. R., *An Introduction to Dynamic Meteorology*, 319 pp., Academic Press, San Diego, Calif., 1972.
- Holton, J. R., *The Dynamic Meteorology of the Stratosphere and Mesosphere*, 216 pp., Am. Meteorol. Soc., Boston, Mass., 1975.
- Jensen, E. J., O. B. Toon, L. Pfister, and H. B. Selkirk, Dehydration of the upper troposphere and lower stratosphere by subvisible cirrus clouds near the tropical tropopause, *Geophys. Res. Lett.*, **23**, 825-828, 1996.
- Jensen, E. J., L. Pfister, A. S. Ackerman, and O. B. Toon, How effectively can freeze-drying by optically thin, laminar cirrus dehydrate air rising slowly across the tropical tropopause?, *J. Geophys. Res.*, in press, 2000.
- Karoly, D. J., G. L. Rolf, and M. J. Reeder, Gravity-wave activity associated with tropical convection detected in TOGA-COARE sounding data, *Geophys. Res. Lett.*, **23**, 261-264, 1996.
- Kelly, K. K., M. H. Proffitt, K. R. Chan, M. Loewenstein, J. R. Podolske, S. E. Strahan, J. C. Wilson, and D. Kley, Water vapor and cloud water measurements over Darwin during the STEP 1987 tropical mission, *J. Geophys. Res.*, **98**, 8713-8723, 1993.
- Koop, T., H. P. Ng, L. T. Molina, and M. J. Molina, A new optical technique to study aerosol phase transitions: The nucleation of ice from H<sub>2</sub>SO<sub>4</sub> aerosols, *J. Phys. Chem.*, **102**, 8924-8930, 1998.
- Liou, K. N., S. C. Ou, Y. Takano, F. P. J. Valero, and T. P. Ackerman, Remote sounding of tropical cirrus cloud temperatures and optical depth using 6 micron and 10.5 micron radiometers during STEP, *J. Appl. Meteorol.*, **29**, 716-726, 1990.
- McFarquhar, G. M., A. J. Heymsfield, J. Spinhirne, and B. Hart, Thin and subvisual tropopause tropical cirrus: Observations and radiative impacts, *J. Atmos. Sci.*, **57**, 1841-1853, 2000.
- Mergenthaler, J. L., A. E. Roche, J. B. Kumer, and G. A. Ely, Cryogenic limb array etalon spectrometer observations of tropical cirrus, *J. Geophys. Res.*, **104**, 22,183-22,194, 1999.
- Mote, P. W., et al, An atmospheric tape recorder: The imprint of tropical tropopause temperatures on stratospheric water vapor, *J. Geophys. Res.*, **101**, 3989-4006, 1996.
- Murphy, D. M., D. S. Thomson, and M. J. Mahoney, In-situ measurements of organics, meteoritic materials, mercury, and other elements in aerosols at 5 to 19 kilometers, *Science*, **282**, 1665-1669, 1998.
- Newell, R. E., Y. Zhu, E. V. Browell, S. Ismail, W. G. Read, J. W. Waters, K. K. Kelly, and S. C. Liu, Upper tropospheric water vapor and cirrus: Comparison of DC-8 observations, preliminary UARS Microwave Limb Sounder measurements and meteorological analyses, *J. Geophys. Res.*, **101**, 1931-1941, 1996.
- O'Sullivan, D., and T. J. Dunkerton, Generation of inertia-gravity waves in a simulated life cycle of baroclinic instability, *J. Atmos. Sci.*, **52**, 3695-3716, 1995.
- Potter, B., and J. R. Holton, The role of monsoon convection in the dehydration of the lower tropical stratosphere, *J. Atmos. Sci.*, **52**, 1034-1050, 1995.
- Rosenfield, J. E., D. B. Considine, M. R. Schoeberl, and E. V. Browell, The impact of subvisible cirrus clouds near the tropical tropopause on stratospheric water vapor, *Geophys. Res. Lett.*, **25**, 1883-1886, 1998.
- Rossow, W. B. and R. A. Schiffer, ISCCP cloud data products, *Bull. Am. Meteorol. Soc.*, **72**, 2-20, 1991.
- Sassen, K., M. K. Griffin, and G. C. Dodd, Optical scattering and microphysical properties of subvisible cirrus clouds, and climatic implications, *J. Appl. Meteorol.*, **28**, 91-98, 1989.
- Schoeberl, M., and L. C. Sparling, Trajectory modelling, diagnostic tools in atmospheric science, *Proc. Int. School of Phys.*, 289-305, 1995.
- Schubert, S. D., and R. Rood, An assimilated dataset for earth science applications, *Bull. Am. Meteorol. Soc.*, **74**, 2331-2342, 1993.
- Sherwood, S. C., On moistening of the tropical troposphere by cirrus clouds, *J. Geophys. Res.*, **104**, 11,949-11,960, 1999.
- Tuck, A., et al, The Brewer-Dobson circulation in the light of high altitude in situ aircraft observations, *Q. J. R. Meteorol. Soc.*, **123**, 1-69, 1997.
- Wang, P. H., P. Minnis, M. P. McCormick, G. S. Kent, and K. M. Skeens, A 6-year climatology of cloud occurrence frequency from stratospheric aerosol and gas experiment II observations (1985-1990), *J. Geophys. Res.*, **101**, 29,407-29,429, 1996.
- Winker, D. M., and C. R. Trepte, Laminar cirrus observed near the tropical tropopause by LITE, *Geophys. Res. Lett.*, **25**, 3351-3354, 1998.

E. V. Browell and W. B. Grant, Chemistry and Dynamics Branch, NASA/Langley Research Center, MS 401A, Hampton, VA 23691-2199. (E.V.Browell@larc.nasa.gov; W.B.Grant@larc.nasa.gov)

T. P. V. Bui, and L. Pfister, Atmospheric Chemistry and Dynamics Branch, NASA/Ames Research Center, MS 245-5, Moffett Field, CA 94035-1000. (pbui@mail.arc.nasa.gov; pfinder@telsci.arc.nasa.gov)

B. Gary, 333 Old Mill Road #225, Santa Barbara, CA 93110. (bruce1gary@home.com)

E. Hints, Department of Marine Chemistry and Geochemistry, Woods Hole Oceanographic Institution, Woods Hole, MA 02543. (ehints@whoi.edu)

E. J. Jensen, Atmospheric Physics Branch, NASA/Ames Research Center, MS 245-4, Moffett Field, CA 94035-1000. (ejensen@sky.arc.nasa.gov)

M. J. Mahoney, Microwave and Lidar Technology Section, Jet Propulsion Laboratory, MS 246-101,

4800 Oak Grove Drive, Pasadena, CA 91109-8099. (Michael.J.Mahoney@jpl.nasa.gov)

H. B. Selkirk, Space Physics Research Institute, 572 Hyannis Drive Sunnyvale, CA 94087. (hselkirk@mail.arc.nasa.gov)

M. R. Schoeberl, Code 910, NASA/Goddard Space Flight Center, MS 916.0, Greenbelt, MD 20771. (schom@ze-phyr.gsfc.nasa.gov)

Owen B. Toon, Laboratory for Atmospheric and Space Physics, Campus Box 392, University of Colorado, Boulder, CO 80309. (toon@lasp.colorado.edu)

(Received March 16, 2000; revised August 15, 2000; accepted August 29, 2000.)